CENTRO DE INVESTIGACIONES EN ÓPTICA, A.C.

CENTRO DE INVESTIGACIONES EN ÓPTICA A.C.

INTEGRATED NANOPHOTONIC WAVEGUIDE LATTICES AS PHOTONIC QUANTUM SIMULATORS

T H E S I S

THIS DISSERTATION IS SUBMITTED IN PARTIAL FULFILLMENT
OF THE REQUIREMENTS FOR THE DEGREE OF:

Master in Sciences (Optics)

PRESENTS:

Juan Samuel S. Durán Gómez

THESIS ADVISOR:
Dr. Roberto Ramírez Alarcón

León, Guanajuato, México

September 2019

To Emily Durán, Cristina Gómez, Alberto Padilla, specially Valentina Padilla and everyone those with a well defined goal.

Acknowledgements

I would like to express my sincere gratitude towards the people whose support throughout the last two years has made this work possible.

Firstly, I am indebted with my advisor, Dr. Roberto Ramírez Alarcón. Since bachelor student until today he has supported me, he accepted me in his group of research and the advices for my professional and personal development.

I would like to thanks to Dr. Rafael Salas Montiel for accept the internship and for all the new knowledge provided in order to improve my professional development.

I am grateful with my fiends and researchers at CIO for the knowledge, tine and experiences shared during the master.

I am so much grateful with my friends of France who helped me a lot during the internship
Finally, I am deeply grateful with my parents and my daughter, this achievement belongs to them for all the time, support and patient in this career.

Declaration of authenticity

I hereby declare that this work is constituted by my authorship, except when specific reference is made to the work of other people. The content of this thesis is original and has not been fully or partially presented for any other degree in this or any other study center. This thesis is the result of my own work and does not include anything that is the result of any work done in collaboration, unless specifically indicated in the text.

Juan Samuel S. Durán Gómez.
León, Guanajuato, México.
September 2019.

Contents

List of Figures

List of Tables

Chapter 1

Introduction

1.1 Overview, motivation, and challenges

Quantum information science recently emerges as a science that could provide a great impact in modern society due to the direct application in quantum technologies (QT).The implementation of QT will provide solutions to many problems and challenges encountered in quantum computation, communications, simulation, metrology, sensing, and imaging [1–4]. Such technologies take advantage of the properties and phenomena encountered in quantum mechanics particularly, in quantum optics.

Quantum simulators have attracted considerably attention in recent years as they have the potential to solve many problems that are hard to solve with current computers [5]. Quantum simulators aim at mimic other quantum systems but with the ability to manage the parameters of the system (Fig. 1.1). The dynamics of the simulator is designed to match the time evolution of the model system to be simulated. In an analog simulator, this is achieved by matching the dynamics of the simulator with the time evolution governing the dynamics of the simulated model. In a digital simulator, the propagator describing the dynamical evolution is constructed from a series of quantum gates [6]. Within the systems considered for the implementation of a practical and suitable platform for quantum computing and simulation, quantum photonics has been considered as one of the most promising candidate, as it can be applied in a large variety on quantum information applications and can be implemented with current CMOS[1] technology, in contrast to other quantum physical systems such as cold atoms and trapped ions [7, 8].

Furthermore, photons are considered as the ideal carrier of information due to the high transmission data speed, low decoherence and information losses. Quantum bits, represented as any physical two-level quantum system, can be encoded in the polarization state of photons and can be therefore manipulated. Path and other degrees of freedom can be used to encode quantum information. Photonic quantum technology has been used to simulate problems in quantum chemistry, biology, and solid-state physics [5, 9].

For instance, integrated optical waveguide lattices were theoretically proposed to investigate and mimic the atom–field interaction. By a proper transformation of the atom–field Hamiltonian and the selection of the initial state for the atom–field wavefunction, it was demonstrated that differential equations that governs this interaction is equivalent to the

[1] complementary metal-oxide-semiconductor

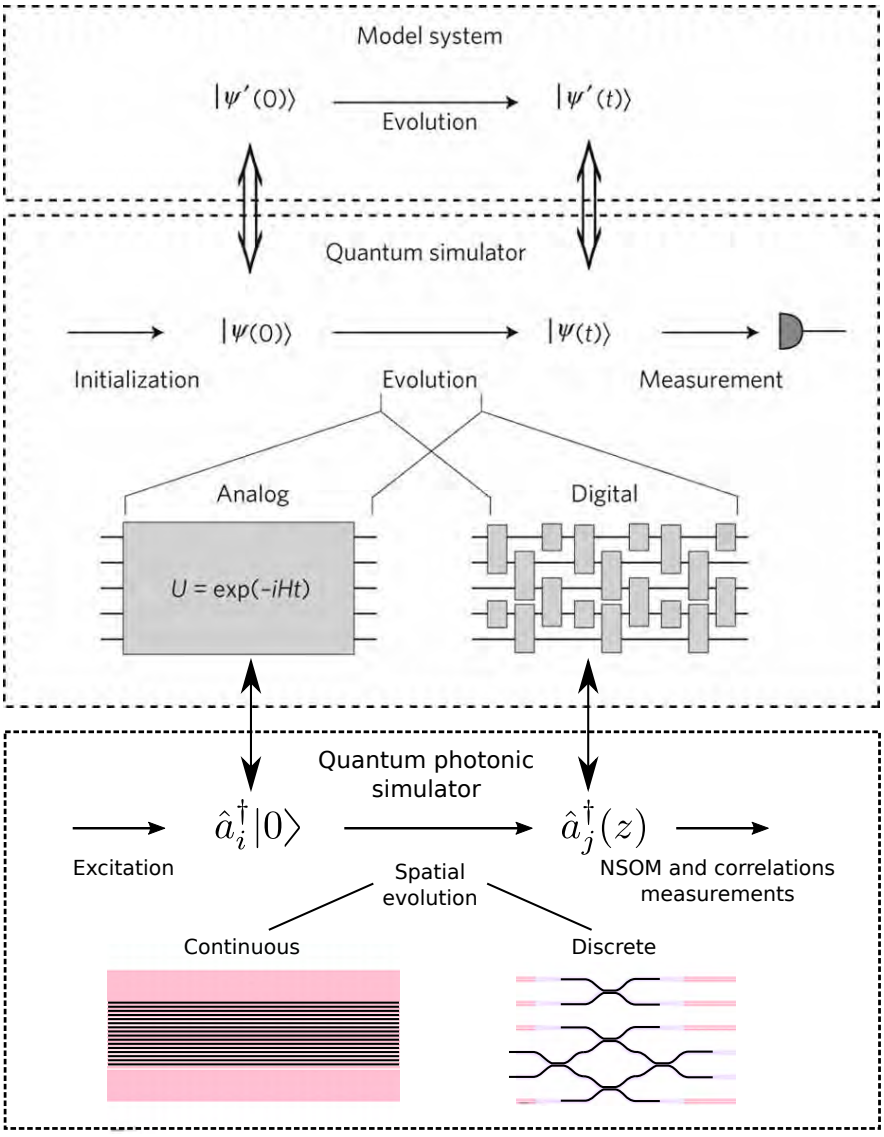

Figure 1.1: Principle of quantum simulators. The are tree steps in a quantum simulator: preparation of the input state, time evolution over a time t and carrying out measurements on the evolved state to extract the physical information of interest. Image taken and adapted from [**?**]. Quantum photonic is a technology able to efficiently implement quantum simulator.

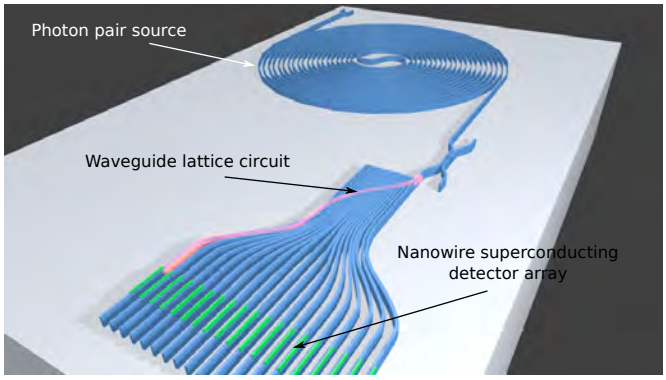

Figure 1.2: Schematic of an integrated nanophotonic quantum simulator. Nanofabrication advances allow the implementation and the integration of single-photon sources, circuits, and high-efficiency superconductor nanowire detection arrays on a single-chip.

study of "diatomic" waveguide arrays [10]. In the last citation is shown the quantum interaction between a two-level atom with a quantized field that can be modelled using photonic lattices for a direct observation the dynamics of the quantum system.

Integrated photonic circuits can also be used to develop other specific quantum tasks such as quantum walks [11, 12], coherent transport of quantum states [13], Glauber-Fock states [14], two-site Bose–Hubbard model [15], Bloch oscillations [16, 17] , and Anderson localization [18, 19].

The fabrication and miniaturization of photonic circuits is one of the most important problems for quantum integrated technologies. It has been demonstrated that femtosecond (fs) laser writing allow the fabrication of optical waveguides with a few microns of size [1, 20, 21]. However, direct fs laser written waveguides are limited in size by the optical diffraction limit of the lenses. This limit can be overtaken with the use of electron beam lithography writing technique [22–24]. Current advances in nanofabrication allow to foresee the implementation of quantum simulators with integrated nanophotonics. In general, integrated nanophotonics serve as an excellent platform for the generation, manipulation, and detection of photons (Fig. 1.2) [24, 25].

In this Master thesis research work, we focus on the implementation of quantum systems on integrated nanophotonic waveguide lattices based on silicon nitride waveguides. With the use of such nanophotonic quantum simulators, tight-binding Hamiltonians mimic a spin chain for perfect transfer of quantum states [13]. We will also mimic Glauber-Fock states in photonic waveguide lattices [14] and the motion of a particle confined in a periodic potential known as Bloch oscillations [26]. We have employed theoretical as well as numerical methods based on finite difference and modal methods implemented by the freely-available MIT Photonic Bands (MPB) and Metric. With Metric, we design and simulate the propagation of light through photonic waveguide arrays that mimic a particular

quantum system. We engineer the interaction between optical mode in waveguide lattices based on the coupled mode theory.
Although the objective of the thesis is the simulation of physical systems with numerical methods, we additionally fabricated the quantum photonic simulator with an array of silicon nitride nanophotonic waveguides.

This work is developed within the framework of a recent collaboration established between the *Université de Technologie de Troyes, France* and *Centro de Investigaciones en Óptica A.C., Mexico*. One of the specific goal of the collaboration is to coupled micro- and nano-photonic circuits to develop the next-generation of high fiber coupling efficiency with integrated quantum nanophotonic circuits.

1.2 Scientific objectives

Our primary aim is to design and fabricate integrated nanophotonic waveguide lattices that constitute the building block for the development of quantum photonic simulators. These quantum nanophotonic simulators allow investigation of many interesting phenomena in other quantum systems. Specifically, we plan to develop an integrated nanophotonic circuit based on nanophotonic waveguide lattices on silicon nitride platform that imitates quantum system encountered in solid-state physics.
To achieve this purpose, we fixed the following specific objectives:

1.2.1 Specific objectives

- To theoretically study the dynamics of common quantum systems and to translate them into photonic coupled waveguide systems.
- We plan to employ the coupled mode theory for the study and implementation of the photonic coupled waveguide array.
- We will use numerical simulations based on finite difference and modal methods to investigate the dispersion relations of waveguides and the propagation of light along the waveguide lattices. This numerical methods are already implemented in freely-available software MIT photonic band (MBP) for eigenmode calculations and Metric for the simulation of electromagnetic light propagation.
- We plan to fabricate the nanophotonic circuits with electron beam lithography and reactive ion etching processes.

1.3 Scope and organization of the thesis

The scope of the manuscript was to provide the design and electromagnetic modeling of quantum simulators based on nanophotonic waveguide lattices. The photonic lattice consist of an array of coupled silicon nitride photonic waveguides.

This thesis manuscript is divided into four chapters.
In the Chapter 2, we describe the theoretical formulation for optical waveguides, a brief review on quantum mechanics, the coupled mode theory and the Hamiltonian formulation for photonic lattices as follows:

- Mathematical description of optical waveguides using Maxwell's equations to find the effective index of the waveguides and the spatial distribution of the mode for planar and ridge waveguide.
- Coupled mode theory as a description for the physical system formed with two optical waveguides in order to define the coupling constant, length of coupling due to this parameters have importance for the design of integrated photonic circuits.
- A revision of the most important concepts in quantum mechanics used in the definition of states and evolution for optical waveguide arrays
- Hamiltonian Formulation for optical waveguide arrays where the dynamics of the system is related with the propagation along the waveguide arrays

We describe, in Chapter 3, silicon nitride as a dielectric material used for the development and implementation of optical waveguides. We show the simulation of two coupled waveguides and the calculation to determine the coupling coefficient. Once determined the function for the coupling constant, it is possible to design basic integrated devices as directional couplers, CNOT gate and the optical lattices involved in this thesis. The correspondent simulations for every systems are shown in every subsection respectively.

Followed this, in Chapter 4 we present the most representative techniques used recently in the manufacture process of optical waveguides for micro and nano platforms. We also discuss the advantages and disadvantages of every technique and we describe the full process to manufacture the devices previously designed and simulated.

Finally, we present the conclusions of the present work, some interesting points in the development of this kind of devices and future work for this project.

Chapter 2

Fundamentals of optical waveguides and quantum systems

2.1 Introduction

This chapter introduces the theoretical fundamental concepts in quantum optics and optical waveguides that are relevant to this research work. It begins with the description of Maxwell's equation in dielectric media. The theoretical formulation of the wave equation as a linear transformation, especially as an operator (i.e. as an eigenvalue problem) is presented. The fundamental properties of optical modes and coupled mode theory are also presented in this chapter. The analytical solution of the wave equation in planar and ridge optical waveguides is presented in appendix A.

We also introduced the theoretical elements of the physical systems that we proposed to simulate and implement with photonic waveguide lattices. The elements of quantum optics such as Fock and coherent states encountered in quantum mechanical systems are presented. The last point presented in this chapter is the tight-binding approximation that is used in our quantum simulator. The Hamiltonian formulation for optical waveguide arrays is shown at the end of the chapter. In summary, this chapter presents the theoretical framework to be considered in subsequent chapters.

2.2 Maxwell's equations in dielectric media

Macroscopic Maxwell equations are used to describe the propagation of electromagnetic fields in dielectric and metallic media. The macroscopic Maxwell's equations are given by [27, 28]:

$$\nabla \cdot \tilde{\mathbf{D}}(\mathbf{r}, t) = \rho, \tag{2.1}$$

$$\nabla \cdot \tilde{\mathbf{B}}(\mathbf{r}, t) = 0, \tag{2.2}$$

$$\nabla \times \tilde{\mathbf{E}}(\mathbf{r}, t) = \frac{\partial}{\partial t}\tilde{\mathbf{B}}(\mathbf{r}, t), \tag{2.3}$$

$$\nabla \times \tilde{\mathbf{H}}(\mathbf{r}, t) = \vec{\mathbf{J}} + \frac{\partial}{\partial t}\tilde{\mathbf{D}}(\mathbf{r}, t), \tag{2.4}$$

where $\tilde{\mathbf{D}}(\mathbf{r},t)$ is the displacement field, $\tilde{\mathbf{E}}(\mathbf{r},t)$ the macroscopic electric field, $\tilde{\mathbf{H}}(\mathbf{r},t)$ the macroscopic magnetic field, and $\tilde{\mathbf{B}}(\mathbf{r},t)$ the magnetic induction field. For a dielectric material, the absence of free charges or currents impose $\rho = 0$ and $\vec{\mathbf{J}} = 0$. The displacement field is related to the electric field, while the induction magnetic field to the magnetic field with the following constitutive equations:

$$\tilde{\mathbf{D}}(\mathbf{r},t) = \varepsilon_0 \varepsilon(\mathbf{r}) \tilde{\mathbf{E}}(\mathbf{r},t), \tag{2.5}$$

$$\tilde{\mathbf{H}}(\mathbf{r},t) = \frac{1}{\mu_o \mu(\mathbf{r})} \tilde{\mathbf{B}}(\mathbf{r},t), \tag{2.6}$$

where ε_0 is the permittivity and μ_o the permeability of vacuum. ε is the dielectric function of the material, generally this function depends of the position and frequency.

Rewriting the Maxwell's equations and using vectorial identities, we obtain the wave equation for the electric and magnetic fields in dielectric media:

$$\nabla^2 \tilde{\mathbf{E}}(\mathbf{r},t) - \mu_0 \varepsilon_0 n^2 \frac{\partial^2}{\partial t^2} \tilde{\mathbf{E}}(\mathbf{r},t) + \nabla \left(\frac{\nabla \varepsilon(\mathbf{r})}{\varepsilon(\mathbf{r})} \cdot \tilde{\mathbf{E}}(\mathbf{r},t) \right) = 0, \tag{2.7}$$

where $\varepsilon = n^2$ and c is the speed of light, defined as $c = (\mu_o \varepsilon_0)^{-1/2}$ [27, 28]. The equation (2.7) is the general wave equation in the electric field form. For the magnetic field, we obtain:

$$\nabla^2 \tilde{\mathbf{H}}(\mathbf{r},t) - \mu_0 \varepsilon_0 \frac{\partial^2}{\partial t^2} \tilde{\mathbf{H}}(\mathbf{r},t) + \frac{1}{\varepsilon(\mathbf{r})} \nabla \varepsilon(\mathbf{r}) \times (\nabla \times \tilde{\mathbf{H}}(\mathbf{r},t)) = 0. \tag{2.8}$$

Because Maxwell's equations are linear, time and space dependency can be separated by expanding the fields into a set of **harmonic modes**. We can therefore write the fields as a spatial pattern times a complex exponential as:

$$\tilde{\mathbf{E}}(\mathbf{r},t) = \mathbf{E}(\mathbf{r})\, e^{-\mathrm{i}\omega t} \tag{2.9}$$

$$\tilde{\mathbf{H}}(\mathbf{r},t) = \mathbf{H}(\mathbf{r})\, e^{-\mathrm{i}\omega t}. \tag{2.10}$$

The last equation mean, we do not know the spatial distribution of the fields in the media, but it is possible to solve the temporal part using separation of variables.
Taking into consideration harmonic modes and using equations (2.4) and (2.3), we obtain the following equation for the magnetic field:

$$\boxed{\nabla \times \left(\frac{1}{\varepsilon(\mathbf{r})} \nabla \times \mathbf{H}(\mathbf{r}) \right) = \left(\frac{\omega}{c} \right)^2 \mathbf{H}(\mathbf{r}).} \tag{2.11}$$

Equation (2.11) is known as the **master equation**. A series of operations act over the magnetic field and if $\mathbf{H}(\mathbf{r})$ is an allowed mode, the result is a scalar multiplied by the original function $\mathbf{H}(\mathbf{r})$.

2.2.1 Electromagnetism as an eigenvalue problem

The left hand side term in the equation (2.11) can be seen as an operator acting on the mode profile $\mathbf{H}(\mathbf{r})$, so we can rewrite it as [29]:

$$\hat{\mathbf{\Theta}}\mathbf{H}(\mathbf{r}) = \left(\frac{\omega}{c}\right)^2 \mathbf{H}(\mathbf{r}), \tag{2.12}$$

where the operator $\hat{\mathbf{\Theta}}$ is defined by:

$$\hat{\mathbf{\Theta}}\mathbf{H}(\mathbf{r}) = \nabla \times \left(\frac{1}{\varepsilon(\mathbf{r})}\nabla \times \mathbf{H}(\mathbf{r})\right). \tag{2.13}$$

We observe that the action of the operator is: first to take the curl to the vector, then divide by $\varepsilon(\mathbf{r})$ and finally take the curl to the result. This treatment can be also applied for the electric field, in this case we have used the magnetic field due to mathematical convenience. The eigenvectors $\mathbf{H}(\mathbf{r})$ are the spatial patterns of the modes and the eigenvalues $(\omega/c)^2$ are proportional to the square of the frequency of those modes. The operator $\hat{\mathbf{\Theta}}$ is a linear operator and Hermitian, which implies specific properties that we will present in the following sections.

2.2.1.1 Fundamental properties of eigenmodes

The operator $\hat{\mathbf{\Theta}}$ and the vectors fulfills important properties, which are of great utility is the description of the modes. We can observe that the operator $\hat{\mathbf{\Theta}}$ is a *linear operator*, that is, if we find the solutions $\mathbf{H}_1(\mathbf{r})$ and $\mathbf{H}_2(\mathbf{r})$ for the master equation, then, a linear combination of both solutions is also a solution for the master equation, that is, $\alpha\mathbf{H}_1(\mathbf{r}) + \beta\mathbf{H}_2(\mathbf{r})$, where, α and β, are constants related with the probabilities amplitude of each mode.

The operator $\hat{\mathbf{\Theta}}$ also is an *Hermitian Operator*, this is an important characteristic, where $\hat{\mathbf{\Theta}}$ satisfies the following properties.

- The eigenvalues of $\hat{\mathbf{\Theta}}$ are positive real values, in such a way that, $\omega > 0$.
- $\hat{\mathbf{\Theta}} = \hat{\mathbf{\Theta}}^\dagger$, that is, the operator is equal to the transposed conjugate.

In addition to Hermicity, $\hat{\mathbf{\Theta}}$ forces any two harmonic modes with difference frequencies ω_1 and ω_2 to have inner product of zero, that it:

$$(\omega_1^2 - \omega_2^2)\langle \mathbf{H}_1(\mathbf{r}), \mathbf{H}_2(\mathbf{r})\rangle = 0. \tag{2.14}$$

If $\omega_1 \neq \omega_2$, then $\langle \mathbf{H}_1(\mathbf{r}), \mathbf{H}_2(\mathbf{r})\rangle = 0$ and the modes are orthogonal. However if $\omega_1 = \omega_2$, then the modes are degenerate and not necessarily orthogonal.

2.2.2 Coupled mode theory

The electromagnetic field in a waveguide forms a complete system of orthogonal functions. This means, any field can be represented as a superposition of modal electromagnetic fields [28]. We consider electromagnetic fields with different supported modes, for the spatial part we have the equations (2.15) and (2.16), represented mathematically as follows [29, 30]:

$$\mathbf{E}\left(x,y,z\right)=\sum_{\nu}a_{\nu}(z)\mathbf{E}_{\nu}\left(x,y\right)e^{-\mathrm{i}\beta_{\nu}z} \tag{2.15}$$

$$\mathbf{E}\left(x,y,z\right)=\sum_{\mu}a_{\mu}(z)\mathbf{E}_{\mu}\left(x,y\right)e^{-\mathrm{i}\beta_{\mu}z}. \tag{2.16}$$

Using equations (2.4), (2.3) and equations (2.15) and (2.16), we obtain the coupled equation for waveguides supporting different modes described by:

$$\frac{\mathrm{d}a_{\mu}(z)}{\mathrm{d}z}=\pm\mathrm{i}\sum\kappa_{\mu\nu}\left(z\right)a_{\nu}\left(z\right)e^{-\mathrm{i}(\beta_{\nu}-\beta_{\mu})z}, \tag{2.17}$$

where $\kappa_{\mu\nu}(z)$ is denoted as the coupling constant for the ν and μ modes.

The equation (2.17) describes the energy exchanges between the fields propagation along of the coupled waveguides, this is considered as a new electromagnetic system with a new restrictions. To obtain the energy exchange between optical waveguides is necessary that the waveguides are closer to each other in such a way the evanescent waves overlap between them [31]. Considering the coupling coefficient independent of the propagation distance, it means, $\kappa_{\mu\nu}\neq\kappa_{\mu\nu}(z)$ and assuming that the waveguides just can carry the fundamental mode, the optical waveguides have the same characteristics (refractive index, size of the waveguide, morphology), such that, $\beta_{\nu}=\beta_{\mu}$.

We can assume that the energy exchange only occur between neighbor waveguides, for which we obtain the following coupled mode equations [32, 33]:

$$\frac{\mathrm{d}a_{n}}{\mathrm{d}z}=\pm\mathrm{i}\kappa_{n}(a_{n+1}\left(z\right)+a_{n-1}\left(z\right)), \tag{2.18}$$

where n represents the n-th waveguide. Here thus, the first waveguide only interact with the second waveguide and in the same way, the n-th waveguide only interacts with the $(n-1)$-th waveguide. Equation (2.18) is a system of first order differential equations coupled, for which $n>2$ becomes difficult to solve analytically. The calculation of the coupling constant is difficult to obtain.

To solve the two coupled mode equation, we first need to write the coupled system of differential equations for two waveguides, in the equations (2.19) and (2.20), $A(z)$ and $B(z)$ represents the complex amplitude for the first and second waveguides respectively.

$$\mathrm{i}\frac{\mathrm{d}A\left(z\right)}{\mathrm{d}z}+\kappa\ B\left(z\right)=0 \tag{2.19}$$

$$\mathrm{i}\frac{\mathrm{d}B\left(z\right)}{\mathrm{d}z}+\kappa\ A\left(z\right)=0. \tag{2.20}$$

The last system of differential equation can be solved analytically with proper initial conditions, $A(0)=1$ and $B(0)=0$. We found the solutions:

$$A\left(z\right)=\cos\left(\kappa z\right) \tag{2.21}$$

and

$$B\left(z\right)=\mathrm{i}\sin\left(\kappa z\right). \tag{2.22}$$

With the last description is possible to measure the coupling constant using the equation (2.23), where $I_A=|A(z)|^2$ and $I_B=|B(z)|^2$, represents the intensity in the waveguide A and B respectively. z is the direction of propagation. The coupling coefficient κ is given by:

$$\kappa=\frac{1}{z}\tan^{-1}\sqrt{\frac{I_B}{I_A}}. \tag{2.23}$$

The distance at which the first waveguide transferred all the energy to the second waveguide is called the *coupling length (l_c)* and is defined as:

$$l_c=\frac{\pi}{2\kappa}. \tag{2.24}$$

In order to obtain 50:50 of energy in a system of two coupled waveguide, the coupling length has to be:

$$l_{50/50}=\frac{\pi}{4\kappa}. \tag{2.25}$$

In the same way, we can find the length for different ratios. In the next chapters we show the design for different devices, the two coupled parallel system is known as a directional coupler.

2.2.3 Numerical methods: WMM mode solver and eigenmode expansion

There are many different software used for modeling physical systems based in optical and optoelectronics devices, they can be commercial or free use and each one proves advantages or disadvantages. Every software uses a different method in order to solve the system.

In the development of this thesis we used two freely-available software for simulating optical waveguides: *VEIMS Mode Solver and Wave Matching Method (WMM)* in order to obtain the propagation constant (β), the effective refractive index (n_{eff}) and the width of optical waveguides with a height constant for single mode optical waveguides; and Metric for light propagation in coupled waveguide arrays.

2.2.3.1 WMM Mode Solver

VEIMS mode solver and WMM are two different tools used in the design of the optical waveguides, it can used to find all the eigenmodes allowed in a multilayer system, for a selected mode it shows the effective refractive index and in consequence, the propagation constant. This software also allows to plot of the desired mode.The accuracy of this method relies on the number of spectral terms considered in the calculation which relapse in computing time.

The vectorial effective index method (VEIM) can be viewed as some bridge between two popular approaches, namely the Film Mode Matching (FMM) on the one hand and the effective index method (EIM) on the other [34].

This mode solver is a free software that can be used in any operating system where the main programming language is C++, but it can be implemented only with an interface for easy use.

2.2.3.2 Eigenmode expansion on Metric

The Metric program collection combines a series of semianalytical tools for the simulation and design of structures or devices from integrated optics / photonics. The programs are meant for frequency domain modeling of configurations in two spatial dimensions, with piecewise constant, isotropic, lossless, and preferably rectangular permittivity distributions.

Optical electromagnetic fields are represented by series of eigenmodes associated with 1-D, piecewise constant refractive index profiles. Accordingly, a reasonably robust and general mode solver for dielectric multilayer slab waveguides is found at the center of the tool collection. Apart from standard guided mode analysis, the mode solver routines include facilities for the generation of orthonormal modal basis sets on finite 1-D intervals, where the mode spectrum is discretized by Dirichlet- or Neumann boundary conditions [35].

Metric is a free software that can be used in any operating system where the main programming language is C++ as well, it does not have an interface such that a few knowledge of programming language is required. Metric works in the frequency domain for modeling structures in two spatial dimensions with rectangular structures for medium isotropic and lossless. This tool allows solve a large integrated photonics circuits with rectangular shapes, which is a considerable disadvantage but it can solve with low computing times and resources that make it useful in comparison with other numerical methods.

Metric do not include tools for visualizing the numerical output data. This output data is stored in Matlab Scripts which can be manipulated easy for the user. For more details of these softwares you can visit the following link: https://www.siio.eu

2.3 Basics of quantum optics and quantum logic gates

Taking into account that the electromagnetic field is conformed of single quanta particles called *photons* we need to introduce the concepts for this treatment. In this section we are going to describe the fundamental concepts for quantum optics used for the realization of our quantum simulators and the introduction to the quantum phenomena which relies on the design for the devices.

The most important in a physical system is to find the dynamics and the evolution in time of it, this can be achieved in the Schrödinger equation for a given state $|\Psi\rangle$ as:

$$\mathrm{i}\hbar\frac{\partial\left|\Psi(\mathbf{r},t)\right\rangle}{\partial t}=\hat{H}\left|\Psi(\mathbf{r},t)\right\rangle. \tag{2.26}$$

The time evolution for any operator $\hat{\Theta}$ independent of time can be described in the Heisenberg picture as:

$$\mathrm{i}\hbar\frac{d\hat{\Theta}}{dt}=[\hat{\Theta},\hat{H}] \tag{2.27}$$

Equations (2.26) and (2.27) are going to be of very use in the description of optical arrays of waveguides.

2.3.1 Quantization of the free electromagnetic field

Considering an electromagnetic field confined in a cavity along the z-axis with perfect walls in the points $z=0$ and $z=L$, such the electric field vanish in the boundaries taking the form of a standing wave. With this consideration we can rewrite the Maxwell's equations when there is no sources and currents in the cavity as follows [36]:

$$\nabla\cdot\tilde{\mathbf{E}}(\mathbf{r},t)=0 \tag{2.28}$$

$$\nabla\cdot\tilde{\mathbf{B}}(\mathbf{r},t)=0 \tag{2.29}$$

$$\nabla\times\tilde{\mathbf{E}}(\mathbf{r},t)=-\frac{\partial}{\partial t}\tilde{\mathbf{B}}(\mathbf{r},t) \tag{2.30}$$

$$\nabla\times\tilde{\mathbf{B}}(\mathbf{r},t)=\mu_0\varepsilon_0\frac{\partial}{\partial t}\tilde{\mathbf{E}}(\mathbf{r},t) \tag{2.31}$$

The electric field that satisfy the boundary condition is given by:

$$E_x(z,t)=\left(\frac{2\omega^2}{V\varepsilon_0}\right)^{\frac{1}{2}}q(t)\sin(kz), \tag{2.32}$$

and the magnetic induction field by:

$$B_y(z,t) = \left(\frac{\mu_0\varepsilon_0}{k}\right)\left(\frac{2\omega^2}{V\varepsilon_0}\right)^{\frac{1}{2}} \dot{q}(t)\cos(kz), \tag{2.33}$$

where $q(t)$ is the canonical position, $\dot{q}(t) = p(t)$ is the canonical momentum of a particle with mass unitary and V is the effective volume of the cavity. The total energy of the electromagnetic field can be calculated with the Hamiltonian:

$$\begin{aligned} H &= \frac{1}{2}\int d^3\mathbf{r}\left[\varepsilon_0\mathbf{E}^2(\mathbf{r},t) + \frac{1}{\mu_0}\mathbf{B}^2(\mathbf{r},t)\right] \\ &= \frac{1}{2}\int dV\left[\varepsilon_0 E_x^2(z,t) + \frac{1}{\mu_0}B_y^2(z,t)\right] \end{aligned} \tag{2.34}$$

Substituting Eqs. (2.32) and (2.33) in the equation (2.34), we obtain the Hamiltonian for a classical harmonic oscillator of unit mass described by:

$$H = \frac{1}{2}(p^2 + \omega^2 q^2). \tag{2.35}$$

Taking the advantage of the variables *p* and *q* represent the canonical position and momentum respectively, we can use the rule of correspondence to replace them as operators satisfying the following commutation rule:

$$[\hat{q}, \hat{p}] = \mathrm{i}\hbar. \tag{2.36}$$

Introducing the annihilation and creation operators in terms of the canonical position and momentum operator, we have the following relations:

$$\begin{aligned} \hat{a} &= \frac{1}{\sqrt{2\hbar\omega}}(\omega\hat{q} + i\hat{p}) \\ \hat{a}^\dagger &= \frac{1}{\sqrt{2\hbar\omega}}(\omega\hat{q} - i\hat{p}). \end{aligned} \tag{2.37}$$

This two operators satisfy the commutation relation:

$$[\hat{a}, \hat{a}^\dagger] = 1 \tag{2.38}$$

Using last assumption, the electric and magnetic fields takes the forms of operators as well, they can be written in terms of the annihilation and creation operators as:

$$\begin{aligned} \hat{E}_x(z,t) &= E_0(\hat{a} + \hat{a}^\dagger)\sin(kz) \\ \hat{B}_y(z,t) &= B_0\frac{1}{i}(\hat{a} - \hat{a}^\dagger)\cos(kz) \end{aligned} \tag{2.39}$$

where $E_0 = (\hbar\omega/\varepsilon_0 V)^{1/2}$ and $B_0 = (\mu_0/k)(\varepsilon_0\hbar\omega^3/V)^{1/2}$ represent the electric and magnetic field "per photon". Finally the hamiltonian can be written in terms of the ladder operators as:

$$\hat{H} = \frac{1}{2}(\hat{p}^2 + w^2\hat{q}^2) = \hbar\omega\left(\hat{a}\hat{a}^\dagger + \frac{1}{2}\right). \tag{2.40}$$

2.3.2 Quantization of the electromagnetic field in optical waveguides

For the consideration of the quantum mechanical description of light is necessary the Hamiltonian formulation in a optical waveguide [37]. Restarting from the Maxwell's equations we can calculate the total energy for the electromagnetic field with the real parts of the fields $\mathbf{E}_r = \frac{1}{2}(\mathbf{E}(\mathbf{r}) + c.c.)$ and $\mathbf{B}_r = \frac{1}{2}(\mathbf{B}(\mathbf{r}) + c.c.)$:

$$H = \frac{1}{2}\int d^3\mathbf{r}\left(\varepsilon_0\varepsilon(\mathbf{r})\mathbf{E}_r(\mathbf{r})\cdot\mathbf{E}_r(\mathbf{r}) + \frac{1}{\mu_0}\mathbf{B}_r(\mathbf{r})\cdot\mathbf{B}_r(\mathbf{r})\right) \tag{2.41}$$

As described in equation (2.9), the spatial part of the electric field can be described by $\mathbf{E}(\mathbf{r}) = \mathbf{E}\,(x,y)\,e^{i\beta z}$ and using equation (2.3), we obtain the magnetic induction field. With weakly guided modes ($\beta|\mathbf{E}|$), the Hamiltonian can be rewritten as:

$$H = \frac{1}{8}\int d^3\mathbf{r}(E(x,y)e^{i\beta z} + c.c.)^2\left(\varepsilon_0\varepsilon(\mathbf{r}) + \frac{\beta^2}{\mu_0\omega^2}\right) \tag{2.42}$$

Considering isotropic medium, we can rewrite the dielectric function as a constant and the electric field can be decomposed in its real and imaginary parts:

$$E(x,y) = \omega q(x,y) + ip(x,y). \tag{2.43}$$

Substituting equation (2.43) in (2.42) and taking into account the last consideration, we obtain:

$$H = \frac{1}{8}\left(\varepsilon_0\varepsilon + \frac{\beta^2}{\mu_0\omega^2}\right)\int d^3\mathbf{r}[(\omega q(x,y) + ip(x,y))e^{i\beta z} + c.c.]^2. \tag{2.44}$$

The terms rapidly oscillating in the z-direction vanish, which implies $\int e^{\pm i2\beta z}dz = 0$, approximating the propagation constant $\beta^2 \approx \frac{\omega^2\varepsilon}{c^2}$ and the length of the waveguide as L, we have the following expression:

$$H = \frac{1}{2}\left(\varepsilon_0\varepsilon L\right)\iint[\omega^2q^2(x,y) + p^2(x,y)]dxdy. \tag{2.45}$$

Rewriting $Q^2 = (\varepsilon_0\varepsilon L)\iint q^2(x,y)dxdy$ and $P^2 = (\varepsilon_0\varepsilon L)\iint p^2(x,y)dxdy$, where Q and P represent the conjugates variables, position and momentum, respectively. With this transformation we obtain the Hamiltonian of the classical harmonic oscillator.

$$H = \frac{1}{2}(\omega^2Q^2 + P^2). \tag{2.46}$$

Finally, with the same treatment for the quantization of the classical oscillator, we can rewrite the Hamiltonian using the operators of position and momentum or the annihilation and creation operators showed in the equation (2.47).

$$\hat{H} = \hbar\omega\left(\hat{a}^\dagger\hat{a} + \frac{1}{2}\right). \tag{2.47}$$

In the next subsections many important relations and properties for this operators will be described.

2.3.3 Fock and coherent states

The *number states*, also called *Fock states* $|n\rangle$, are a semi-infinite set of eigenstates of the Hamiltonian operator, where *n* represents the number of photons in the system yielding to:

$$\hat{H}\,|n\rangle = \hbar\omega\left(\hat{n}+\frac{1}{2}\right)|n\rangle = \hbar\omega\left(\hat{n}+\frac{1}{2}\right)|n\rangle\,, \tag{2.48}$$

where we have replaced the number operator $\hat{n} = \hat{a}^\dagger\hat{a}$. These operators satisfy the bosonic commutation relation given by:

$$[\hat{a},\hat{a}^\dagger] = 1. \tag{2.49}$$

The creation and annihilation operators have an operation in the basis of Fock states represented as the generation or destruction of photons:

$$\begin{aligned}\hat{a}^\dagger\,|n\rangle &= \sqrt{n+1}\,|n+1\rangle\\ \hat{a}\,|n\rangle &= \sqrt{n}\,|n-1\rangle\,.\end{aligned} \tag{2.50}$$

The operator $\hat{n}$ is an Hermitian operator, while the destruction and creation operators are not Hermitian but allow a easy treatment in the mathematical analysis in quantum mechanics, quantum optics, and electromagnetism as seen in subsection 2.2.1.

The quantized electromagnetic field can be described using *coherent states* ($|\alpha\rangle$), which were first proposed by Glauber [38]. A coherent beam of light has associated a field amplitud α with a phase well-defined but with a number of photons undetermined. These states perform an overcomplete basis, where the state $|\alpha\rangle$ can be expanded in terms of the Fock states $|n\rangle$ defined by:

$$|\alpha\rangle = e^{-\frac{|\alpha|^2}{2}}\sum_{n=0}^{\infty}\frac{\alpha^n}{\sqrt{n!}}\,|n\rangle\,, \tag{2.51}$$

where α is a complex number and the coherent states are expanded into the basis of Fock states. We can observe these states do not form an orthogonal base. Another remarkable properties of these kind of states are:

$$\begin{aligned}\hat{a}\,|\alpha\rangle &= \alpha\,|\alpha\rangle\\ \langle\alpha|\,\hat{a}^\dagger &= \alpha^*\,\langle\alpha|\\ \langle\alpha|\alpha\rangle &= 1\\ \langle\alpha|\hat{a}^\dagger\hat{a}|\alpha\rangle &= |\alpha|^2.\end{aligned} \tag{2.52}$$

Another definition for these states involves the displacement of the vacuum state. The displacement operator for a variable α is defined as:

$$\hat{D}(\alpha) = e^{\alpha\hat{a}^\dagger-\alpha^*\hat{a}}, \tag{2.53}$$

where the coherent state is given by:

$$|\alpha\rangle = \hat{D}(\alpha)\,|0\rangle\,. \tag{2.54}$$

Another form to represent the displacement operator, which facilities the operations, is:

$$\hat{D}(\alpha) = e^{-\frac{|\alpha|^2}{2}} e^{-\alpha^* \hat{a}} e^{\alpha \hat{a}^\dagger}. \tag{2.55}$$

The displacement operator is a unitary operator, however this operator is not Hermitian.

Fock states and coherent states are descriptions of the electromagnetic field that we are going to use in the quantum simulator of Glauber-Fock states.

2.3.4 Two-photon interference

The Hong Ou Mandel effect (HOM) is a pure quantum effect that occurs when two indistinguishable photons arrives at the same time in a beam splitter (BS) promoting quantum interference, it was first demonstrated in 1987 [36, 39]. Considering a BS with R and T corresponding with the reflectivity and transmitivity of the BS respectively, the matrix associated is [36, 40]:

$$BS = \begin{pmatrix} T & R \\ R & -T \end{pmatrix}. \tag{2.56}$$

Remembering $\hat{a}_j^\dagger$ for j=1,2,3,4 as the creation operators for the input and the output modes in the BS; these operators satisfy the rules of bosonic commutation:

$$\begin{aligned} \left[\hat{a}_i^\dagger, \hat{a}_j^\dagger\right] &= 0 \\ [\hat{a}_i, \hat{a}_j] &= 0 \\ \left[\hat{a}_i, \hat{a}_j^\dagger\right] &= \delta_{ij}. \end{aligned} \tag{2.57}$$

The input and outputs relation in function of the BS are described by:

$$\begin{aligned} \hat{a}_3^\dagger &= T\hat{a}_1^\dagger + R\hat{a}_2^\dagger \\ \hat{a}_2^\dagger &= -R\hat{a}_1^\dagger + T\hat{a}_2^\dagger. \end{aligned} \tag{2.58}$$

Now, considering a 50:50 beam splitter, we have R=T=$\frac{1}{\sqrt{2}}$. If we have two indistinguishable photons, each one in one of the input modes at the BS we have the initial state $|\Psi_{12}^{in}\rangle = |1\rangle_1\,|1\rangle_2$ in the basis of Fock states. Using the equation (2.58), we obtain the following output state:

$$|\Psi_{34}^{out}\rangle = \frac{1}{\sqrt{2}}(|2\rangle_3\,|0\rangle_4 + |0\rangle_3\,|2\rangle_4). \tag{2.59}$$

For this output state, the state with one photon on each output mode is suppressed due to bosonic coalescence of photons leading to the *Hong Ou Mandel Effect*. In the figure 2.1 is shown a schematic representation of the HOM effect in a directional coupler.

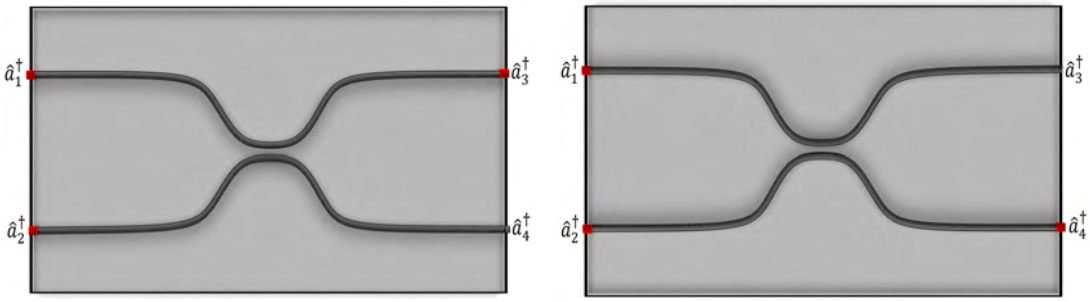

(a) One possibility is to obtain both photons in the output mode $\hat{a}_3^\dagger$.

(b) The second possibility is to obtain both photons in the output mode $\hat{a}_4^\dagger$.

Figure 2.1: Schematic representation of the Hong Ou Mandel Effect. Two indistinguishable photons arrives at the same time in a directional coupler.

2.3.5 Hadamard and CNOT quantum logic gates

The directional coupler is considered one of the main elements in order to develop a task in a quantum photonic circuit. This device is used to divide the optical power in two beams, exploiting the coupling between them with an analogous to the beam splitter in free space.

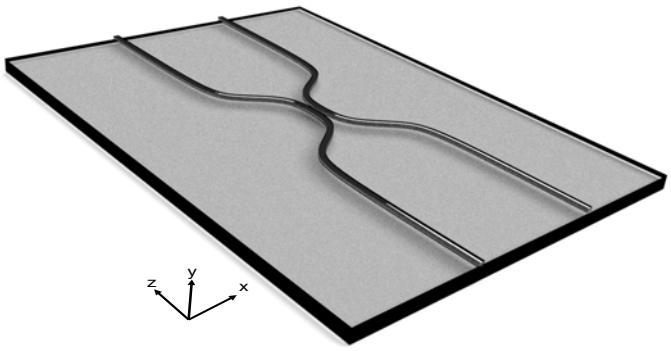

Figure 2.2: Schematic representation of directional coupler. Directional coupled based on ridge waveguides, main element in quantum integrated technologies.

The device is shown in the Fig. 2.2, it consist of two input and output ports separated where no exist energy exchange by evanescent field, then a bend waveguides connect the input ports with central region where two straight waveguides are fixed a certain distance and separation length to obtain energy exchange and finally another bend waveguides connect with the output ports.

Considering the directional coupler as a beam splitter, we can write the following equa-

tions for the power in each arm of the device:

$$\begin{aligned} R &= P_0 \cos^2(\kappa z) \\ T &= P_0 \sin^2(\kappa z), \end{aligned} \tag{2.60}$$

where P_0 is the total power at the input ports, R represents the reflected port and T represents the transmitted port, this definition depends of which one is the input port as a bulk beam splitter.

In quantum computing sciences, the directional coupler acts as a *Hadamard* quantum logical gate for a single photon at the input of the BS. Then, the unitary matrix associated is the same for a 50:50 beam splitter is:

$$H = \mathrm{BS}_{50:50} = \frac{1}{\sqrt{2}} \begin{pmatrix} 1 & 1 \\ 1 & -1 \end{pmatrix}. \tag{2.61}$$

Another important quantum logical gate for quantum computing tasks is the CNOT gate and is the most common two-qubits gate. This quantum logical gate has been demonstrated in free space, fiber optics and integrated photonics, it consist acting over two qubits, the first one called *Control Qubit* and the second one is called *Target Qubit*. This gate flips the target qubit (T) depending on the state of the control qubit (C).
In the computational basis $|00\rangle, |01\rangle, |10\rangle, |11\rangle$, where the first qubit is related with the control qubit and the second qubit is related with the target qubit.

The transformation associated when the CNOT gate acts is:

$$\begin{aligned} |00\rangle &\rightarrow |00\rangle \\ |01\rangle &\rightarrow |01\rangle \\ |10\rangle &\rightarrow |11\rangle \\ |11\rangle &\rightarrow |10\rangle \end{aligned} \tag{2.62}$$

Writing the last states as a column vector we obtain:

$$|00\rangle = \begin{bmatrix} 1 \\ 0 \\ 0 \\ 0 \end{bmatrix}; |01\rangle = \begin{bmatrix} 0 \\ 1 \\ 0 \\ 0 \end{bmatrix}; |10\rangle = \begin{bmatrix} 0 \\ 0 \\ 1 \\ 0 \end{bmatrix}; |11\rangle = \begin{bmatrix} 0 \\ 0 \\ 0 \\ 1 \end{bmatrix} \tag{2.63}$$

Then, the unitary matrix associated with this logical gate is described in the equation (2.64):

$$\hat{U}_{CNOT} = \begin{pmatrix} 1 & 0 & 0 & 0 \\ 0 & 1 & 0 & 0 \\ 0 & 0 & 0 & 1 \\ 0 & 0 & 1 & 0. \end{pmatrix} \tag{2.64}$$

There exists different ways to implement the gate, it means, the qubits can be related with the path [41], or the polarization [42]. In the figure 2.3 is shown a schematic representation of the integrated CNOT gate implemented by path.

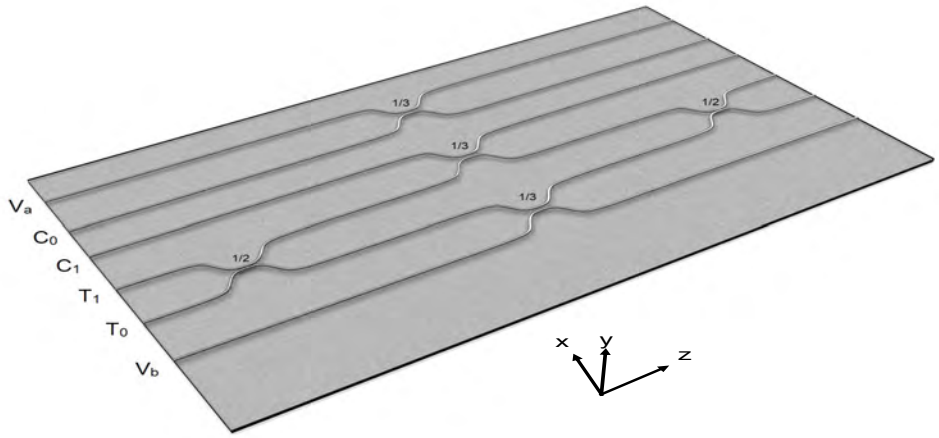

Figure 2.3: Schematic representation of a CNOT quantum logical gate based on integrated photonic circuits.

This gate consist of three directional couplers with reflectivity of $1/3$ located at the center and two 50:50 directional couplers. The gate works as follow: the two $1/2$ directional couplers located at the target ports (T_0 and T_1) forms a balanced Mach-Zehnder interferometer, if we consider no inputs in the control waveguide (or a photon in the control state zero C_0), the photons injected in the target ports exit from the same port as the input port. Now, for the control in state one (photon in the C_1 waveguide), the control and target interfere nonclassically at the central $1/3$ splitter.

For this value of reflectivity the state evolves to $|10\rangle \rightarrow -1/3\,|10\rangle$, causing a π-phase difference in the interferometer, so that the target is flipped.

2.4 Dynamics of quantum systems

In this section we are going to describe three quantum systems, these systems are going to be simulated due to their analogies in the Hamiltonian formulation with the Hamiltonian related to photonic lattices described in the following section.

2.4.1 The Heisenberg spin chain

In quantum technologies a theoretical advances have demonstrated that if coherence can be maintained across many qubits, the transfer of quantum states can be obtained with high performance. The first proposal was to evaluate the state transfer in a spin chain with

a Heisenberg Hamiltonian related [13, 43].

The main idea is the transmission of an initial state from one place to another keeping their properties without losing information, this system has been demonstrated in photonic lattices platform exploiting the similarities with the spin chain system where the coupling can be engineered to achieve the desired task.

The Hamiltonian related to a spin chain of coupled qubits is described by:

$$\hat{H} = \frac{1}{2}\sum_{n=1}^{N-1} J_n(X_n X_{n+1} + Y_n Y_{n+1}). \tag{2.65}$$

where X_n and Y_n represents the Pauli matrices acting on the n-th, N is the total number of sites or qubits involved in the system and J_n is the coupling strength between one to the next site or qubit.

In the following sections and chapter the Hamiltonian comparison and the conditions for the perfect transfer of the quantum state are given.

2.4.2 Glauber-Fock states

Displaced Fock States (DFS) are a generalization of coherent states and have so much importance in quantum optics. These states arise from the displacement of the eigenstates of the harmonic oscillator ($|n\rangle$) and belong to a more general class of states. A few points that make this states attractive are that can be used for a direct measurement of the Wigner function, or they constitute the eigenstates for Jaymes-Cumming model for coherently driven atoms [**?**, 44].

A physical system of coupled waveguides allows a direct observation of a classical analogue of DF engineering the coupling constant as s square root of the number of waveguide. This system is known as Glauber-Fock photonic lattice where an excited waveguide represents a Fock state and the spatial evolution in the optical array corresponds to the probability amplitudes of the DFS in the number basis [45].

One important observation is that we can obtain the same equation of coupled mode theory for waveguides with the same propagation constant if we make the following treatment:

$$a_n(z) = \langle n|\hat{D}(\mathrm{i}\rho \mathrm{z})|k\rangle\,. \tag{2.66}$$

where ρ represents a positive constant, in this context is related with the coupling constant and z represents the propagation distance. Then, calculating the first derivative for the last equation:

$$\frac{d}{dz}a_n(z) = \langle n|\frac{d}{dz}\left(\hat{D}(\mathrm{i}\rho \mathrm{z})\right)|k\rangle\,, \tag{2.67}$$

where we use the properties of coherent states and Fock states previously presented yielding to the coupled equation:

$$\mathrm{i}\frac{da_n(z)}{dz} + \rho(\sqrt{n}a_{n-}(z) + \sqrt{n+1}a_{n+1}(z)) = 0. \tag{2.68}$$

Compare to equation (2.18), we find the coupling constant must be $\kappa_n = \rho\sqrt{n} = \kappa_1\sqrt{n}$ in order to achieve the desired evolution in the system.

2.4.3 Bloch oscillations in solid-state physics

Bloch oscillations are a physical phenomenon when a particle submitted to a periodic potential describes a periodic motion, originally was studied in the context of solid state physics for the study of the dynamics of electrons in crystals. This phenomenon has been of so much interest due to exposes the wave nature of matter [16, 17].

This phenomenon has already been demonstrated in atom lattices, photonic lattices and electronic systems [17, 46, 47]. There are many advantages in the election of a platform to observe it. Photonic lattices is considered one of the most relevant platforms due to the versatility to engineer the artificial potentials modifying the properties of the optical waveguides [48].

There are different descriptions for the Hamiltonian associated, in photonic lattices the propagation constant play the role of the potential [26].

$$\hat{H} = \frac{\hbar c}{n}\sum_{j=1}^{N}\left[\beta_j\hat{n}_j - \kappa(\hat{a}_{j+1}^{\dagger}\hat{a}_j + \hat{a}_j^{\dagger}\hat{a}_{j-1})\right]. \tag{2.69}$$

where $\beta_j$is the propagation constant of every waveguide, $\hat{n}_j = \hat{a}_j^{\dagger}\hat{a}_j$ is the number operator, κ is the coupling constant and $\hat{a}_j^{\dagger}$ and $\hat{a}_j$ are the creation and annihilation operators respectively which represent the mode in the $j-th$ waveguide.

One principal requirement to achieve Bloch oscillations is the coupling strength between waveguides. which has to be constant.

In the following section and chapters we describe the full conditions and parameters to obtain Bloch oscillations in our photonic lattices.

2.5 Photonic waveguide lattices

The Hamiltonian related to three different quantum systems was described in section 2.4. In the following section is described the Hamiltonian for coupled waveguides and its properties Hamiltonian.

2.5.1 Hamiltonian formulation for photonic waveguide lattices

The total Hamiltonian related for an optical waveguide array will be the sum of the Hamiltonian of each waveguide.

Generally the optical waveguides can be different between them if we change the physical shape, it means, the modes allowed and the propagation constant (β_k). For this case and using equation (2.47), we can rewrite the following total Hamiltonian:

$$\hat{H} = \hbar \sum_{k=1}^{N} \omega_k \left(\hat{a}_k^\dagger \hat{a}_k + \frac{1}{2} \right). \tag{2.70}$$

Taking in consideration the approximation $\beta_k^2 \approx \frac{\omega_k^2}{c^2}\varepsilon$, where all the waveguides have the same dielectric constant and $n = \sqrt{\varepsilon}$, yields to:

$$\hat{H} = \frac{\hbar c}{n} \sum_{k=1}^{N} \beta_k \left(\hat{a}_k^\dagger \hat{a}_k + \frac{1}{2} \right). \tag{2.71}$$

However, this Hamiltonian describes arrays of isolated waveguides, in another words, the waveguides are not close enough to evanescent wave coupling. In the tight-binding model, we consider the neighbor waveguide as a perturbation such that enables the coupling between waveguides allowing the energy exchange [26, 31, 49]. With this assume we can rewrite the Hamiltonian as:

$$\hat{H} = \frac{\hbar c}{n} \sum_{k=1}^{N} \left[\beta_k \left(\hat{a}_k^\dagger \hat{a}_k + \frac{1}{2} \right) + \sum_{l=1}^{N} \kappa_{k,l} \hat{a}_k^\dagger \hat{a}_l \right], \tag{2.72}$$

where $\kappa_{k,l}$ is the coupling constant between the k-th and l-th waveguide.

The annihilation and creation operators maintain the following rules for the different modes:

$$[\hat{a}_k, \hat{a}_l^\dagger] = \delta_{k,l} \tag{2.73}$$

and

$$[\hat{a}_k, \hat{a}_l] = [\hat{a}_k^\dagger, \hat{a}_l^\dagger] = 0. \tag{2.74}$$

The number of photons in the waveguides is now tracked in Fock state basis $|n_1, ..., n_N\rangle$ as:

$$\begin{aligned} \hat{a}_k^\dagger |n_1, ..., n_k, ..., n_N\rangle &= \sqrt{n_k + 1}\, |n_1, ..., n_{k+1}, ..., n_N\rangle \\ \hat{a}_k |n_1, ..., n_k, ..., n_N\rangle &= \sqrt{n_k}\, |n_1, ..., n_{k-1}, ..., n_N\rangle . \end{aligned} \tag{2.75}$$

The last Hamiltonian considers coupling between all the waveguides yielding a difficult calculation. In the following chapters, we restrict this Hamiltonian for a particular cases in order to solve it.

2.5.2 Time evolution in photonic lattices

The evolution of the system is best described in the Heisenberg picture, where the states remain invariant, but the operators evolves in time. Using Heisenberg equation (2.27),

$$\mathrm{i}\hbar\frac{d\hat{a}_m^\dagger}{dt} = \mathrm{i}\frac{\hbar c}{n}\frac{d\hat{a}_m^\dagger}{dz} = [\hat{a}_m^\dagger, H], \tag{2.76}$$

where we have replaced the phase velocity along the waveguide as $\frac{dz}{dt} = \frac{c}{n}$ and used the chain rule $\frac{d\hat{a}_m^\dagger}{dt} = \frac{d\hat{a}_m^\dagger}{dz}\frac{dz}{dt}$.

Substituting the Hamiltonian (2.72) into equation (2.76), evaluating the commutator and using the commutation properties for the annihilation and creation operators, we obtain:

$$\mathrm{i}\frac{d}{dz}\hat{a}_m^\dagger(z) + \beta_m\hat{a}_m^\dagger(z) + \sum_{k=1}^{N}\kappa_{k,m}\hat{a}_k^\dagger(z) = 0. \tag{2.77}$$

There are two cases that we are going to restrict: in the first case we consider that all the waveguides have the same dimensions and in the second case, waveguides with different dimensions.

For the first case, the modes have similar propagation constant $\beta_m = \beta_0 + \gamma_m$, where β_0 is an average value and γ_m is a detunning. We introduce a new operator defined as $\hat{b}_m^\dagger = \hat{a}_m^\dagger e^{-\mathrm{i}\beta_0 z}$ to reduce the form of the differential equation. The detunning is absorbed into the coupling matrix as $\tilde{\kappa}_{k,m} = \gamma_k\delta_{k,m} + \kappa_{k,m}$.

$$\mathrm{i}\frac{d}{dz}\hat{b}_m^\dagger(z) + \sum_{k=1}^{N}\tilde{\kappa}_{k,m}\hat{b}_k^\dagger(z) = 0. \tag{2.78}$$

Equation (2.78) involves the coupling between all the waveguides, in order to reduce the complexity of the physical system, we consider that the m-th waveguide just interacts with the neighbor waveguides $(m+1)$-th and $(m-1)$-th, yielding to:

$$\mathrm{i}\frac{d}{dz}\hat{b}_m^\dagger(z) + \tilde{\kappa}_{m+1}\hat{b}_{m+1}^\dagger(z) + \tilde{\kappa}_m\hat{b}_{m-1}^\dagger(z) = 0, \tag{2.79}$$

where $\tilde{\kappa}_{m+1}$ is the coupling constant between the waveguide $m-th$ and $(m+1)-th$ while $\tilde{\kappa}_m$ is the coupling constant between the waveguide $m-th$ and $(m-1)-th$. Equation (2.79) is used for the quantum coherent transport of states and Glauber-Fock state systems.

For the second case, we consider that all waveguides have different propagation constant. This consideration is achieved with the variation of the dimensions but, the waveguides just interact with their neighbor waveguides as in the previous case.
We write therefore the equation of motion as:

$$\mathrm{i}\frac{d}{dz}\hat{a}_m^\dagger(z) + \beta_m\hat{a}_m^\dagger(z) + \kappa_m\hat{a}_{k-1}^\dagger(z) + \kappa_{m+1}\hat{a}_{k+1}^\dagger(z) = 0. \tag{2.80}$$

Finally, equations (2.79) and (2.80) are the equations of motion used for the three quantum photonic simulators in this work. In the following chapter, we mentioned the equation of motion of every system.

2.6 Conclusion

In the present chapter, we provided the background needed and the basis for the transformation of quantum system into array of coupled waveguides. We presented the fundamentals of optical waveguides and the time evolution of quantum system in physics, particularly in solid-states physics, quantum optics, and quantum information (i.e. quantum logic gates). The macroscopic Maxwell's equations for a isotropic and lossless medium were also presented as these equations govern the propagation of light in photonic waveguides and devices. The fundamental properties of eigenmodes were presented in the section electromagnetic as a linear operation.
The numerical tools used for the electromagnetic simulation of coupled waveguide were presented. a brief review of their advantages and disadvantages was presented.

We shown the total Hamiltonian of coupled waveguides, which was used for the design of quantum photonic simulators.

In conclusion, the time evolution of the presented quantum can be indeed mapped into a spatial evolution along the direction of propagation in photonic waveguide lattices.

Chapter 3

Implementation of physical systems with quantum photonic waveguide lattices

3.1 Introduction

In this chapter is described the operation of the integrated photonic circuits, previously to the process of fabrication. Specially we show the unitary operator for the CNOT gate and finally we show the Hamiltonian for every lattice of waveguides and the coupled differential equation, respectively. For every device, we show the simulations performed on Metric software for the propagation along the integrated device.

3.2 Silicon nitride photonic waveguides

The first step for the design of more complex circuits is the design of single mode optical waveguides. For this step we have used VEIMS and WMM solver. We considered the refractive index of silicon nitride as $n_{Si_3N_4} = 2.1$, the refractive index of the cover as the air $n_{cover} = n_{air} = 1$ and the refractive index of the substrate as $n_{substrate} = 1.5$.
For these values of the refractive index of the waveguide, we have fixed the height of the waveguide as $h =$ 300 nm due to the samples had that film value, we looked for single mode optical waveguide for two different wavelengths: 1550 nm and 800 nm. We found that for $\lambda =$ 800 nm the width of the waveguide must be $w =$ 500 nm and for $\lambda =$ 1550 nm the width of the waveguide must be $w = 1\mu$m in order to propagate just the fundamental mode related with the $TE_{0,0}$ mode. These values are very important to be considered in the mask layout design and the manufacture process.

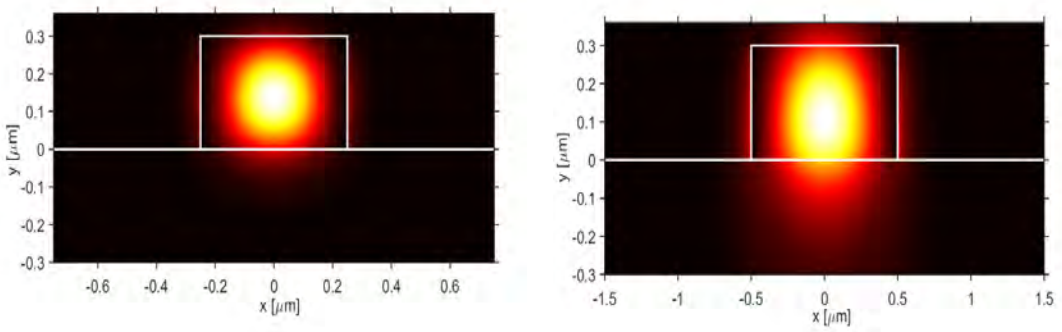

(a) Spatial field distribution for λ = 800 nm, w = 500 nm.

(b) Spatial field distribution for λ = 1550 nm, w = 1000 nm.

Figure 3.1: Calculation of the mode profile for two different wavelength in ridge waveguide for the $TE_{0,0}$ mode for a constant height of h = 300 nm.

In the figure 3.1, we show the spatial mode supported for both wavelengths considered. At the same time we can observe the electromagnetic field concentrated at the center of the waveguide. In the boundaries we can observe a certain part of the electromagnetic field corresponding to the evanescent field.

Previously to the design of another integrated optical devices, we reduced the ridge waveguide to a planar waveguide using the effective index method and finding the following results:

- For λ = 800 nm we have obtained a planar waveguide and based on the figure A.4 for the region I and III we obtained an effective index approximated to the cover, it means, $N_{eff1} = N_{eff3} = 1$, while for region II we have found $N_{eff2} = 1.91515$.
- For λ = 1550 nm, we obtained a planar waveguide and based on the figure A.4 for the region I and III we obtained an effective index approximated to the cover, it means, $N_{eff1} = N_{eff3} = 1$, while for region II we have found $N_{eff2} = 1.7190$

These values and the width of the waveguides for every wavelength are going to be considered in the simulations developed in Metric.

3.3 Directional coupler for two photon quantum interference

Due to the high refractive index of the Si_3N_4, in the curved region there is no exist coupling by evanescent field with the neighbor waveguide. For this reason we consider only energy exchange for the central region where the straight waveguides are located.

Considering the last assumption, many simulations were developed for two coupled waveguides, where the coupling length was obtained as function of separation distance,

after that and using the equation (2.24), the coupling constant κ was recovered and fitted as a exponential function.

In figure 3.2 are shown different pairs of coupled waveguides for $\lambda = 800$ nm , $n_{eff} = 1.91515$ and 500 nm of width in order to determine the coupling constant.

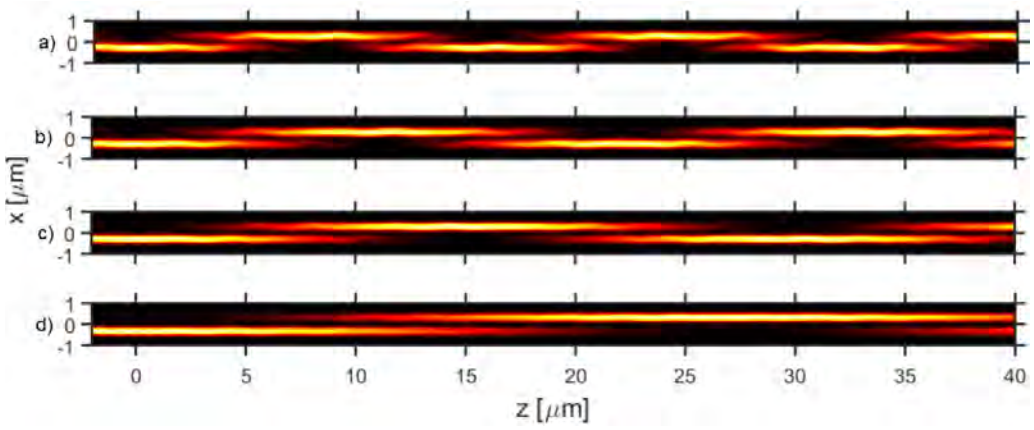

Figure 3.2: Simulation of two coupled waveguides with $\lambda = 800$ nm , $n_{eff} = 1.91515$ w=500 nm varying the separation length for a) $s = 50$ nm, b) s =75 nm, s=100 nm and d) $s = 150$ nm.

We can observe if we increase the separation length we need a higher length propagation to find the coupling length. To determine the coupling constant we have simulated until 300 nm.
The last procedure was realized also for $\lambda = 1550$ nm, $w = 1000$ nm with $n_{eff} = 1.7190$ (Fig. 3.3).

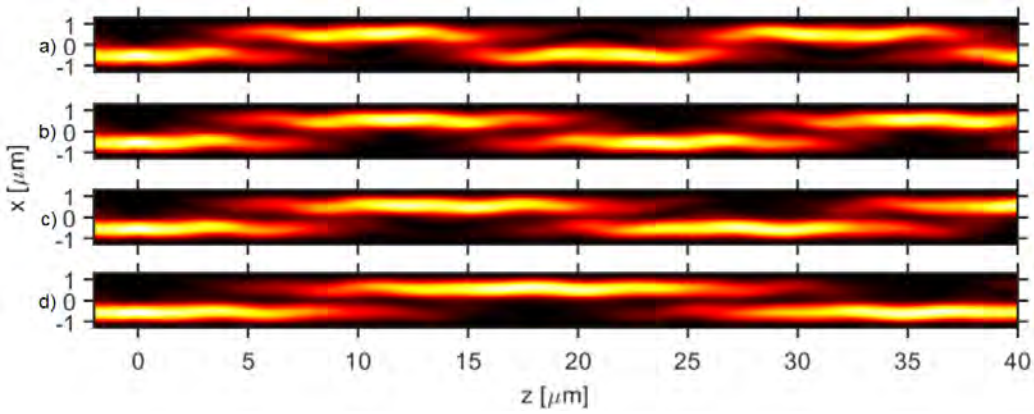

Figure 3.3: Simulation of two coupled waveguides with $\lambda = 1550\ nm$, $n_{eff} = 1.7190$ $w = 1000\ nm$ varying the separation length for a) $s = 50\ nm$, b) $s = 75\ nm$, $s = 100\ nm$ and d) $s = 150\ nm$.

We observed the coupling length for $\lambda = 1550$ nm is less in comparison with $\lambda = 800$ nm, which means the evanescent field is greater.

The coupling constant was fitted to an exponential function of the form:

$$\kappa(s) = \kappa_o e^{-bs}. \tag{3.1}$$

In the figure 3.4 is shown the plot for the coupling constant vs the separation distance for $\lambda = 800$ nm. The exponential function fitted for the coupling constant is $\kappa(s) = 0.3508 \exp^{-0.01195s}$.

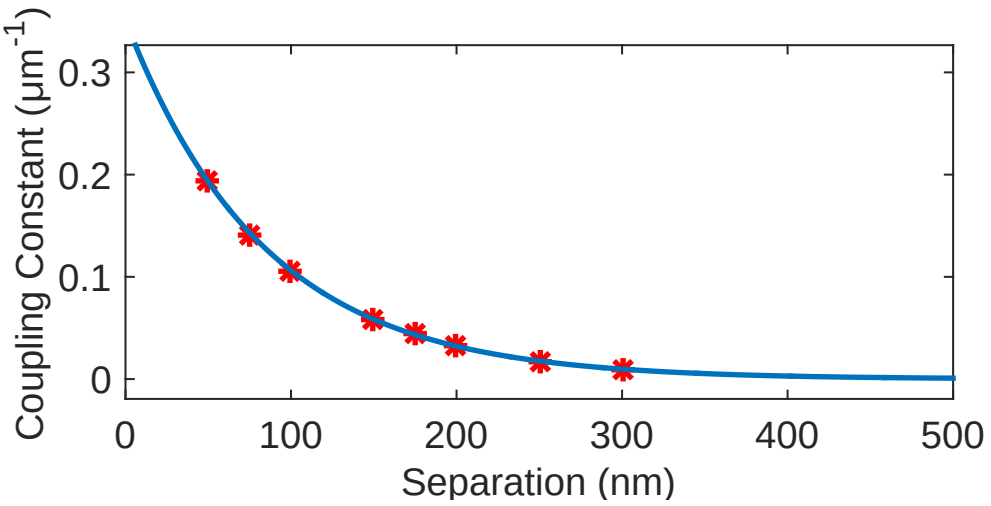

Figure 3.4: The coupling constant in function of the separation distance and fitted to an exponential function. This calculation was developed for $\lambda = 800$ nm.

The same procedure was realized for $\lambda = 1550$ nm, for this case, the function fitted for the coupling constant is $\kappa(s) = 0.1835 \exp^{-0.005089s}$. In the figure 3.5 is shown the plot for the coupling constant vs the separation distance and the fitted function.

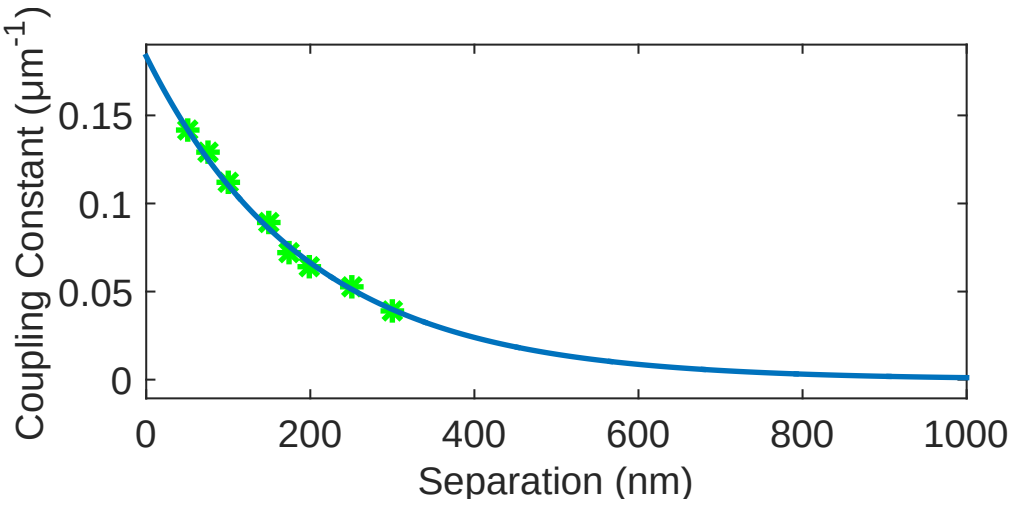

Figure 3.5: The coupling constant in function of the separation distance and fitted to an exponential function. This calculation was developed for $\lambda = 1550\ nm$.

For both cases we observe the coupling constant for two coupled waveguides separated by a distance of 3 μm is almost zero, which is important for the fabrication process.

With the coupling constant known and fitted for every value of separation we can calculate the optimal length to achieve 50:50 directional couplers or any design for directional couplers for a given reflectance or transmittance value.

3.4 Integrated quantum logical gates

In the following subsection are described the parameters used for the design of the CNOT gate, due to the directional coupler acts as a Hadamard gate only using the fitted function we have find the optical distance to create directional couplers with a 50:50 relation for the transmision and reflection ports.

3.4.1 Integrated photonic CNOT gate

For the design of the directional couplers we have selected a fixed separation distance of s = 100 nm. We found the length for 1/2 directional coupler of $l_{1/2} = 7.385\ \mu$m.

For the directional coupler with splitting ratio of 1/3, based on the equations 2.60 we have selected $|R|^2 = \frac{1}{3}$ we have find a length of $l_{1/3} = 8.9784\ \mu$m, All the device was design to work for the wavelength of λ = 800 nm.

3.5 Integrated nanophotonic waveguide lattices

We mentioned above the potential applications of optical waveguide arrays. In the design of the optical waveguide arrays, we used the fitted function for the coupling constant in order to obtain the distance distribution needed for the quantum simulator.

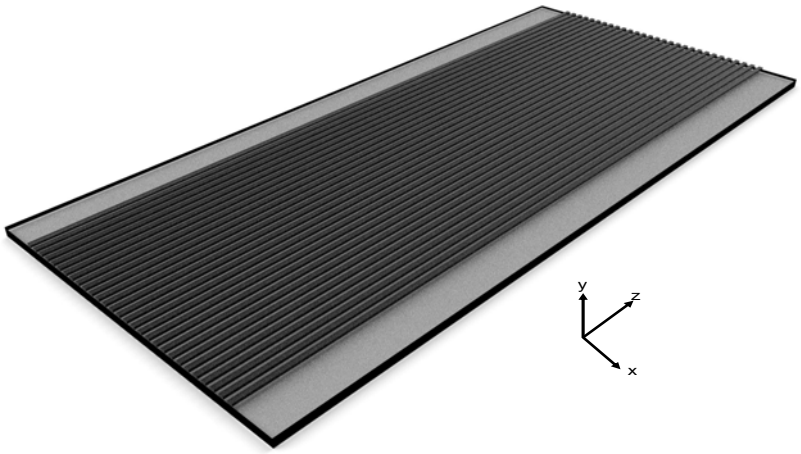

Figure 3.6: Schematic representation of optical photonic lattices based on ridge waveguide.

In the figure 3.6 is shown a 1-D array based on ridge waveguides.

Then, we are going to show the Hamiltonian related with every system, their differential equation and the distance distribution used to achieve the desired system, and the values utilized with their respective simulations on Metric Software.

3.5.1 Quantum coherent transport of states in integrated photonics

Remembering the Hamiltonian associated to obtain the quantum coherent transport of states we have:

$$H = \frac{1}{2}\sum_{n=1}^{N-1} J_n(X_nX_{n+1} + Y_nY_{n+1}). \tag{3.2}$$

Then, the coupled differential equation that satisfies the coupling between neighbor waveguides is described by:

$$i\frac{da_n(z)}{dz} = \kappa_{n+1}a_{n+1}(z) + \kappa_n a_{n-1}(z), \tag{3.3}$$

where $|a_n(z)|^2$ is the probability amplitude to find the photon in the n-th waveguide and z corresponds to the distance of propagation along of the waveguide. For the perfect coherent transport the coupling constant requires a distribution described as:

$$\kappa_n = \frac{\pi\sqrt{n(N-n)}}{2z_f}, \tag{3.4}$$

where z_f is the total length of propagation for the quantum coherent transport of the initial state.

Considering the fitted function for the coupling constant, we rewrite as:

$$\kappa_n(s) = \kappa_1 e^{-(s_n - s_1)/k}, \tag{3.5}$$

where k is a constant, s_n is the distance between the $n-th$ and the $(n+1)-th$ waveguide and s_1 is a reference distance that can be varied in order to achieve the perfect transfer. Substituting equations (3.5) and (2.51), it is possible to find the distance distribution for the spin photonic lattice

$$s_n = s_1 - k\ln\sqrt{\frac{n(N-n)}{N-1}}. \tag{3.6}$$

For the simulation in metric for the wavelength $\lambda = 800$ nm, we used 19 waveguides $s_1 = 250$ nm yielding to the following distance distribution. We observe the distance distribution is symmetric with respect to the central waveguide corresponding to the waveguide number 10.

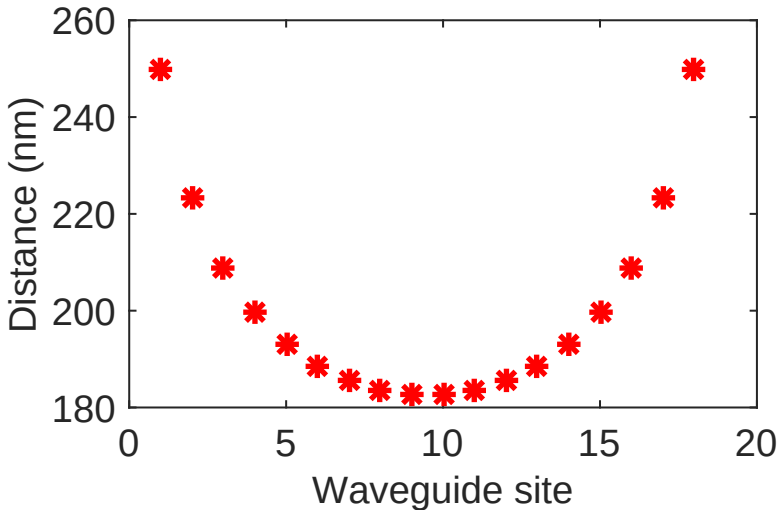

Figure 3.7: Distance distribution for quantum coherent transport of states for the wavelength $\lambda = 800$ nm.

For this distance distribution we find a total length of propagation $z_f = 376.83$ μm.

In the figure 3.8 is shown the simulation of the photonic lattice where we have varied the input state. We have observed the state is perfect transferred to the waveguide $N-n+1$. at the propagation length z_f, when the light is injected into the n-th waveguide.

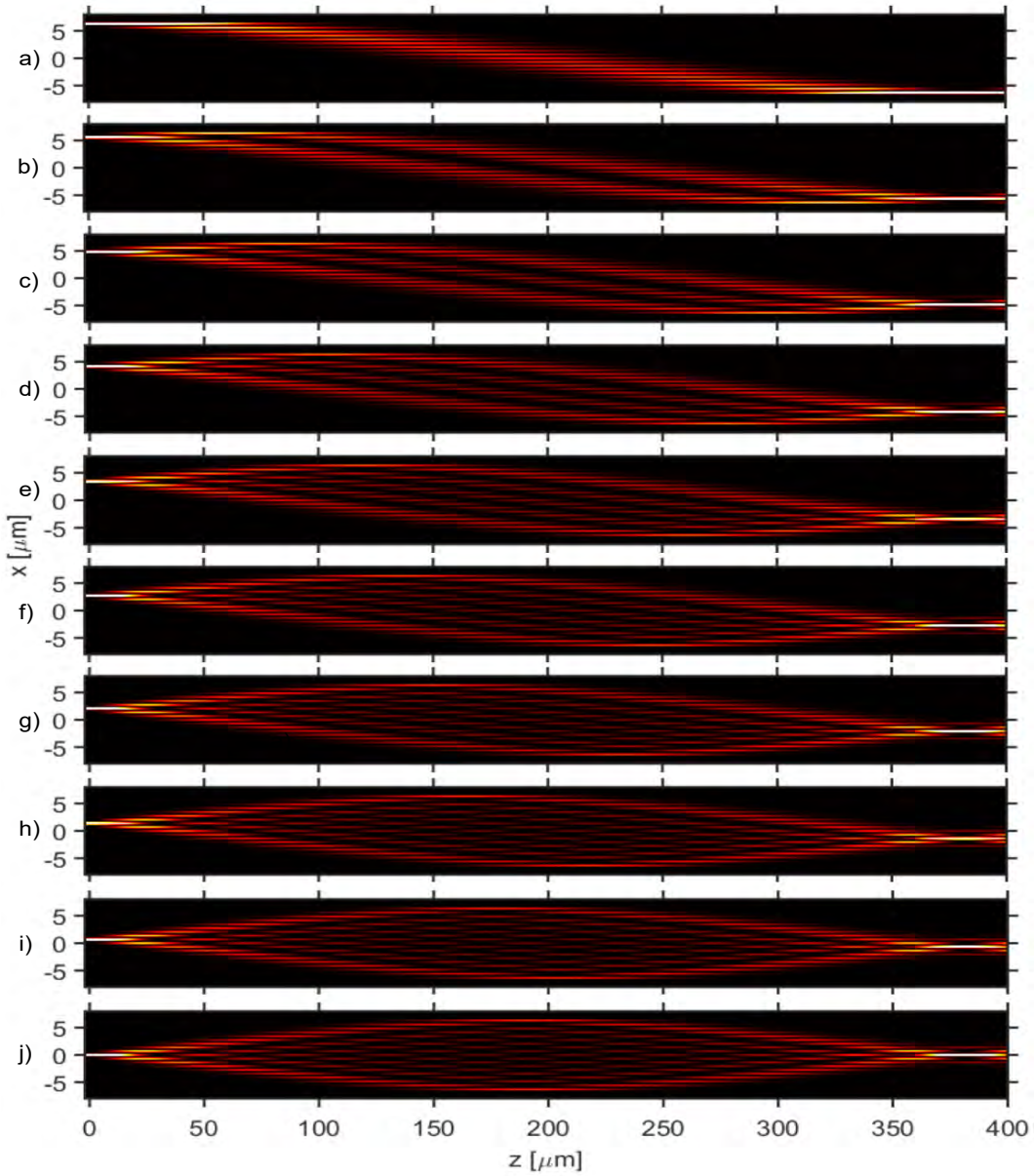

Figure 3.8: Evolution of light in a photonic lattice with 19 waveguides coupled varying the input waveguide for $\lambda = 800$ nm: a) 1, b) 2, c) 3, d) 4, e) 5, f) 6, g) 7, h) 8, i) 9 and j) 10.

In order to observe the dynamics in the photonic lattice and corroborate the quantum coherent transport of both states in the waveguides array, we simulated two photons in the system; in the figure 3.9 is shown two simulations for two different inputs.

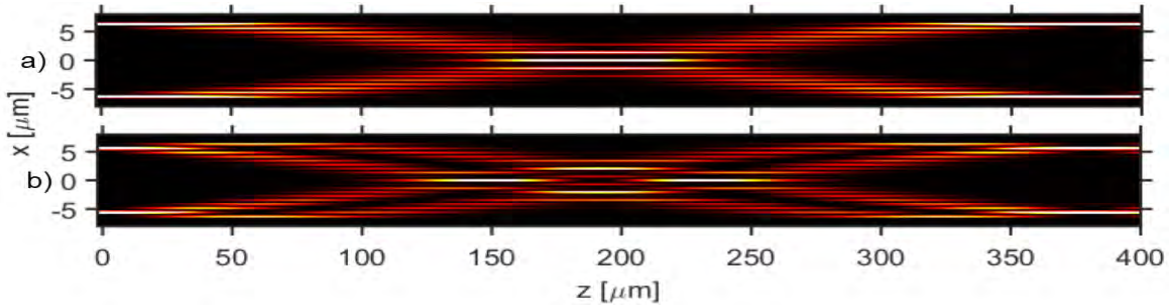

Figure 3.9: Simulation of a photonic lattice with 19 coupled waveguides with two inputs are in the waveguides: a) 1 and 19, b) 2 and 18.

In both cases we observed the output is independent of the number of inputs obtaining the both photons at the calculated length z_f in the output ports related. We also observed an interference pattern in the central region which is different depending of the input ports.

For the wavelength $\lambda = 1550$ nm, we repeated the same procedure in order to achieve the coherent transport of the initial state with 19 waveguides and varying the distance s_1 to find the optimal value for the desired dynamics. We have obtained $s_1 = 600$ nm with a total length of propagation for this device $z_f = 769.47$ μm.

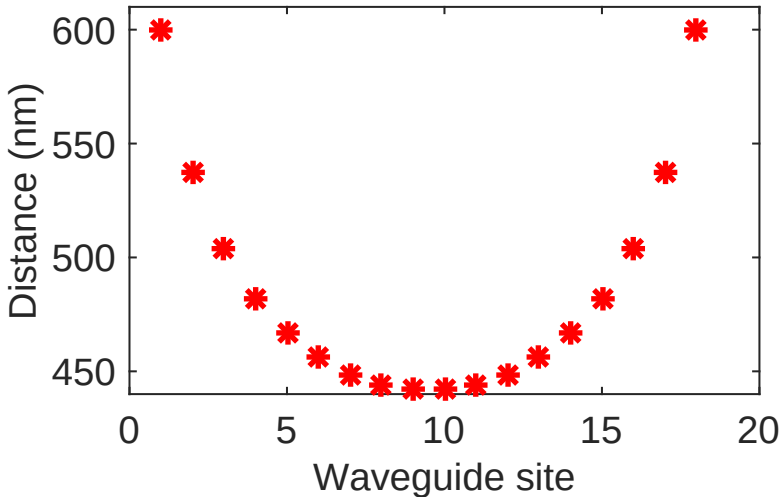

Figure 3.10: Distance distribution for quantum coherent transport of states for the wavelength $\lambda = 1550$ nm.

In the figure 3.10 the distances distribution is shown for the same case, the distance s_n is the distance between the n-th and the $(n+1)$-th waveguide.
The simulation were developed providing the same dynamics as for $\lambda = 800$ nm, but with an increase in the total length of propagation.

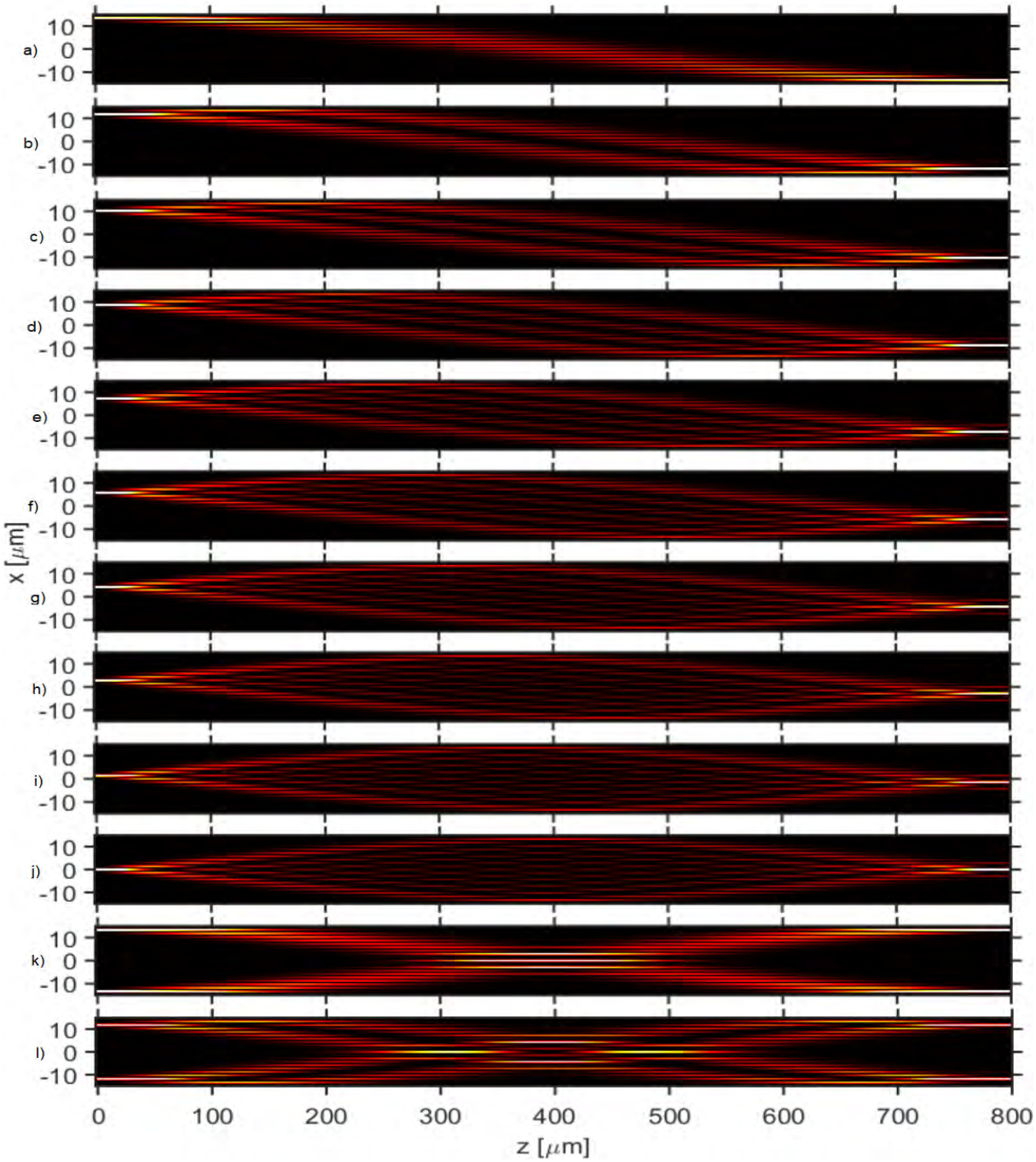

Figure 3.11: Evolution of light in a photonic lattice with 19 waveguides coupled varying the input waveguide for $\lambda = 1550\ nm$: a) 1, b) 2, c) 3, d) 4, e) 5, f) 6, g) 7, h) 8, i) 9, j) 10, k) 1 and 19, l) 2 and 18.

In the figure 3.11 is shown the dynamics in the photonic lattice for $\lambda = 1550$ nm.

It is possible to rewrite the action of the photonic lattice as an unitary matrix that the size of the matrix depends of the number of inputs and outputs. For this case we can rewrite as an unitary square matrix with size of 19 x 19 as:

$$\hat{U} = \begin{pmatrix} 0 & \dots & 0 & 0 & 1 \\ 0 & \dots & 0 & 1 & 0 \\ 0 & \dots & 1 & 0 & 0 \\ \vdots & \ddots & \vdots & \vdots & \vdots \\ 1 & \dots & 0 & 0 & 0 \end{pmatrix} \tag{3.7}$$

In the last matrix all the elements are 0 except the elements located in the secondary diagonal where all the elements has the value of 1.

3.5.2 Glauber-Fock states in integrated photonics

The Hamiltonian related for this system can be written as the same for the photonic lattices where all the waveguides have the same propagation constant:

$$\hat{H} = \frac{\hbar c}{n} \sum_{j=1}^{N} \left[\kappa_n (\hat{a}_{j+1}^{\dagger} \hat{a}_j + \hat{a}_j^{\dagger} \hat{a}_{j-1}) \right]. \tag{3.8}$$

This leads to the following differential coupled equation which is the same previously found with coupled mode theory

$$i \frac{da_n(z)}{dz} = \kappa_1 \sqrt{n+1} a_{n+1}(z) + \kappa_1 \sqrt{n} a_{n-1}(z), \tag{3.9}$$

In order to achieve the desired physical system, we need to fulfill the coupling constant distribution described by:

$$\kappa_n = \kappa_1 \sqrt{n}. \tag{3.10}$$

where this distance distribution can be found substituting equation (3.10) and (3.5) yielding to the following equation:

$$s_n = s_1 - k \ln \sqrt{n}. \tag{3.11}$$

For this simulation it is necessary an array of optical waveguides semi-infinite, physically it is not possible, so that, we used 21 coupled waveguides just to observe the first orders of the Glauber-Fock photonic lattices.

In the figure 3.12 is shown the distance distribution for this system, we observe according to the increase in the n-th waveguide the distance separation s_n between the waveguide n and $n+1$ decreases such while the coupling constant between those waveguides increase.

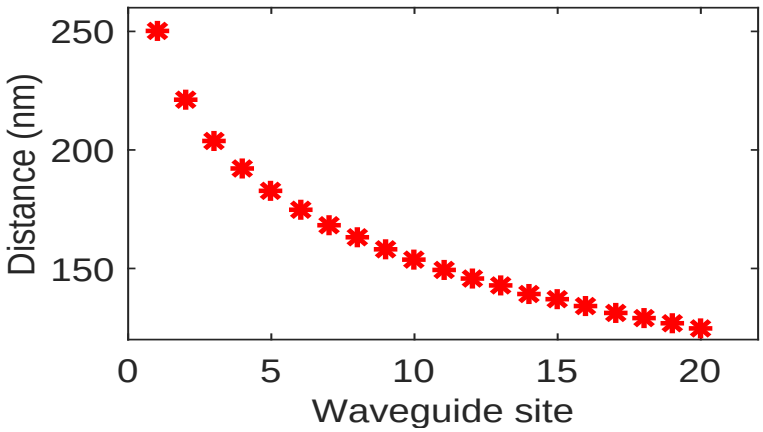

Figure 3.12: Distance distribution for Glauber-Fock states for the wavelength $\lambda = 800$ nm.

In the figure 3.13 is shown the the light evolution in the Glauber photonic lattice for 7 different input ports. Only for this system is considered the first site is represented by $k = n - 1$ where n represents the waveguide excited such the displacement is representede by the state $|k\rangle$.

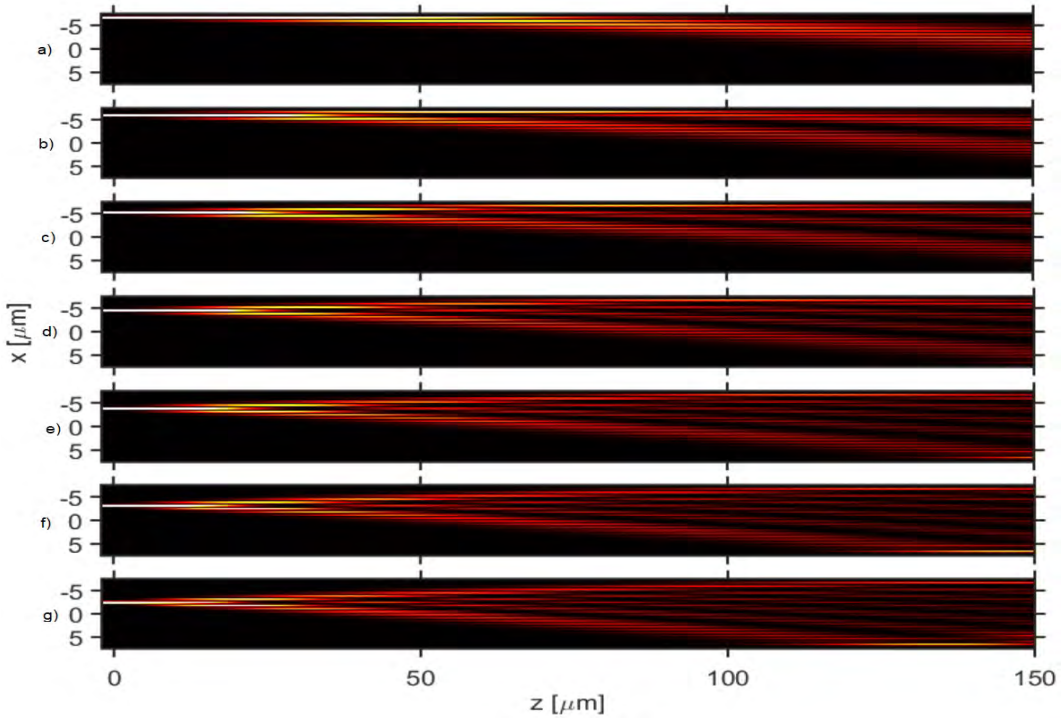

Figure 3.13: Evolution of light in a photonic lattice with 21 waveguides coupled varying the input waveguide for $\lambda = 800$ nm: a) k=0, b) k=1, c) k=2, d) k=3, e) k=4, f) k=5 and g)k=6 representing the displacement of the Fock states $|0\rangle, |1\rangle, |2\rangle, |3\rangle, |4\rangle, |5\rangle, |6\rangle$, respectively.

We can observe depending on the site the lines separated in the pattern evolution of light increase by one.
Using the last distance distribution and a distance of propagation $z_f = 150\ \mu m$ the device was designed for the manufacture process.

3.5.3 Bloch oscillations in integrated photonics

The Hamiltonian associated with this physical system is described by the equation [16, 17, 26]:

$$\hat{H} = \frac{\hbar c}{n} \sum_{j=1}^{N} \left[\beta_k \hat{a}_j^{\dagger} \hat{a}_j - C(\hat{a}_{j+1}^{\dagger} \hat{a}_j + \hat{a}_j^{\dagger} \hat{a}_{j-1}) \right]. \tag{3.12}$$

which leads to the following coupled equation of motion:

$$i \frac{da_n(z)}{dz} = \kappa(a_{n+1}(z) + a_{n-1}(z)) - \beta_n a_n(z), \tag{3.13}$$

In order to obtain Bloch oscillations in our system of coupled waveguides we are going to consider $\beta_n = \beta_0 + \delta\beta_n$. This change of the propagation constant can be achieved in different ways: changing the refractive index of every single waveguide, changing the dimensions of the waveguides or the wavelength for every excited waveguide.
Due to the restrictions for our samples we only can change the width of every waveguide such that makes a change in the propagation constant for the same wavelength.

Firstly, we have calculated the propagation constant using WMM solver starting from $300\ nm$ to $635\ nm$ where all the waveguides supports only fundamental TE and TM modes.
In the figure 3.14 is shown the propagation constant as a function of the width.

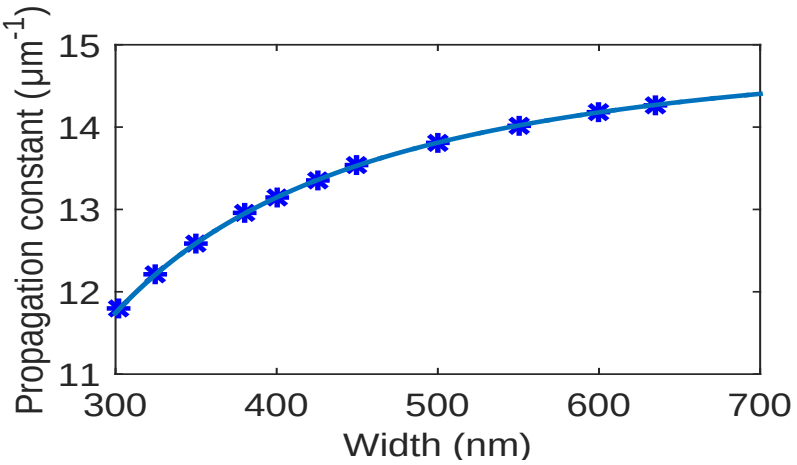

Figure 3.14: Propagation constant as a function of the width.

Using the points calculated with WMM solver we have fitted a function of the form $\beta(w) = aw^b + c$ yielding to:

$$\beta(w) = -0.3316w^{-1.913} + 15.06 \tag{3.14}$$

Then, we have selected an linear increasing for $\delta\beta$ shown in the image 3.15 for 25 waveguides:

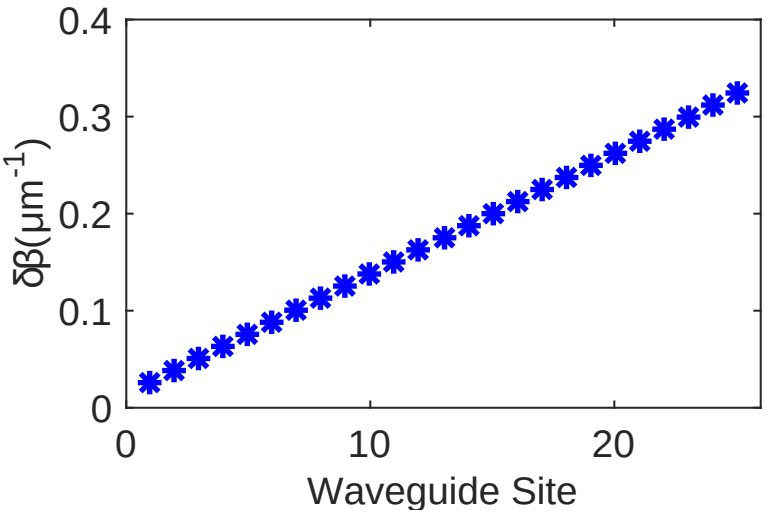

Figure 3.15: Linear increasing as a function of the $n-th$ waveguide.

We have selected an initial value for the propagation constant $\beta_0 = 13.8151$ which correspond to a width of $w = 500\ nm$.

Finally, we can calculate the width of the waveguide in order to obtain a linear increasing for the coupling constant with the equation:

$$w_n = e^{\frac{\ln\left(\frac{\beta_n(w)-c}{a}\right)}{b}} \tag{3.15}$$

which leads to the following width distribution shown in the figure 3.16.

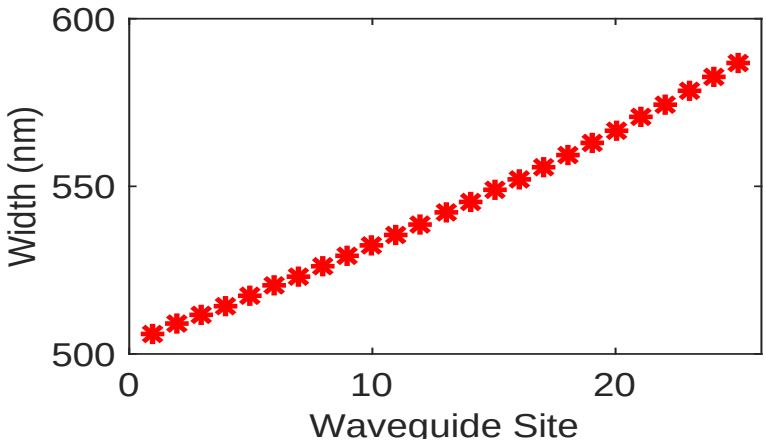

Figure 3.16: Width distribution as a function of the $n-th$ waveguide to achieve Bloch Oscillations in a photonic lattice.

Now, taking into account that the coupling constant must be equal for all the waveguides and remembering that the energy exchange must be only with neighbor waveguides, we have selected a distance constant of 250 nm for all the waveguides due to the width of all the waveguide is around of 500 nm.

In the figure 3.17 is shown the light evolution in the optical photonic lattices where the Bloch oscillations appear.

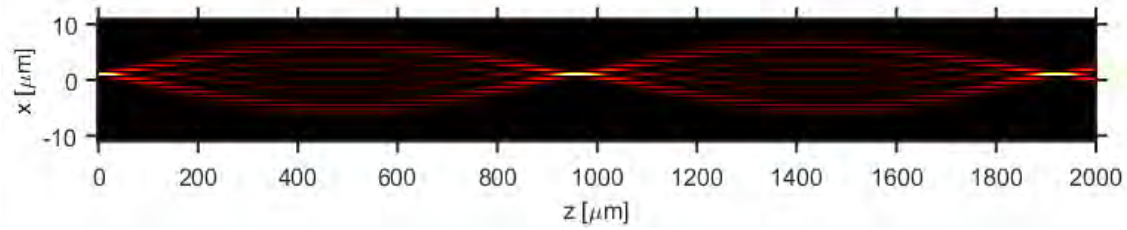

Figure 3.17: Evolution of light in a photonic lattice with 25 waveguides coupled varying the input waveguide for $\lambda = 800$ nm where Bloch oscillations are present.

We observe the light evolves and realize a coherent transport around 980 nm and then the pattern repeats but it does not appear at the double of the first distance.

Using the last values of distance and width we have designed the the mask in order to manufacture de photonic lattice.

3.6 Conclusion

In the present chapter, we presented the design of the photonic quantum simulators based on the time evolution of some quantum systems. Firstly, we designed single mode optical waveguides for the wavelengths 800 nm and 1550 nm with the use of the WMM solver.

Then, using metric solver, we simulated pairs of waveguides with varying separation distance in order to find the function for the coupling constant for both wavelengths 800 nm and 1550 nm. Using the coupling constant function, we designed Hadamard and CNOT gates, two of the most important quantum logical gates.

For the quantum coherent transport of states for the wavelength of $\lambda = 800$ nm and $\lambda = 1550$ nm we have observed the correspondient evolution of light as we predicted but when we injected two photons appeared interesting interference phenomena which needs a more detailed research.

For the quantum simulator of Glauber-Fock states we have observed that a large number of waveguides is necessary in order to develop the desired system, however using a small number of waveguides allows the confirmation of the light evolution in the photonic lattice.

For the quantum simulator of Bloch oscillations we can select the increasing of the propagation constant or the initial propagation constant, such that, the width of the waveguides can be decreased and a large number of waveguides can be allowed to achieve Bloch oscillations.

Finally, we have obtained the desired distance distribution and width distribution for the three quantum systems and we simulated the evolution of light in the optical photonic lattices to develop the quantum simulators. Moreover, Metric and WMM solver are powerful tools that allow the design of systems with high complexity.

Chapter 4

Micro- and nano-fabrication of quantum integrated photonic circuits

4.1 Introduction

In the previous chapters, we detailed the basics and simulations for the design of the integrated photonic quantum simulators that are going to be fabricated. Finally, one of the most important steps for the development of integrated photonic circuits is the nanofabrication process, this chapter starts explaining two different techniques for the fabrication of photonic chips and the rest is dedicated to describe the full process of electron-beam lithography, starting from the preparation of the sample, the pattern design using nanolithography toolbox software and the process to transfer the full pattern to the silicon nitride material. Lastly, we discuss the nanofabrication process and discuss the most relevant points for this chapter.

4.2 Micro- and nano-fabrication techniques

In the following subsections, we describe only two of the common techniques for the fabrication of optical waveguides due to *Centro de Investigaciones en Óptica A.C.* and *Université de Technologie de Troyes*, Francia, have the installations and capabilities to fabrication of them and a brief comparison between the advantages and disadvantages.

4.2.1 Femtosecond laser direct writing

The last years has been demonstrated that the technique of femtosecond laser write is suitable for the manufacture of three dimensional photonic structures within a glass or a crystal [20]. The femtosecond laser micromachining consist in focus a pulsed laser using an objective microscope inside of a transparent material in order to modify the properties of this material due to the high energy focused, it relies on the nonlinear absorption of the material to create an increase of the refractive index in the focal zone and if the sample is translated it is possible to create localized optical buried waveguides.

In the figure 4.1 is shown the representation for the fabrication process of photonic circuits using this technique. Generally, the sample is translated by a xyz micro-positioner,

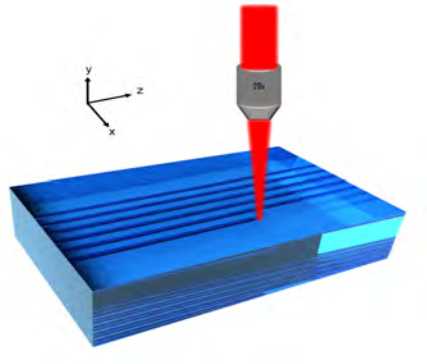

Figure 4.1: Schematic representation of the femtosecond laser writing technique for optical buried waveguides.

allowing so, the fabrication of three dimensional structures in only one step process and enabling the creation of complex circuits.

This technique provides a few potential capabilities in the creation of photonic circuits but also has disadvantages in comparison with another techniques; firstly, the waveguides get a low refractive index contrast, it means, it is easy to create waveguides supporting more modes than the fundamental mode.
Also related with the low refractive index increase, the photonic circuits needs footprints with size in the order of a few centimeters to achieve a task, so, the scalability of the creation chips using this technique is limited by this problem and finally, using this technique we can not manufacture nanophotonic circuits due to the diffraction limit provided by the wavelength of the laser and the numerical aperture of the objective microscope (CIO capabilities).

4.2.2 Electron beam lithography

Electron beam lithography (EBL) is a nanofabrication for many applications in electronics and photonics. EBL is used for the fabrication of single electron devices, electrical connections, ultra-high density storage media and photonic waveguides. The basic principle of EBL is the transfer of a pattern using an electron beam focused at the surface of a e-beam resist. This resist reacts to the electron yielding to a change of physical and chemical properties. At the end, the exposed pattern in the resist is transferred to the material using common techniques like lift-off or reactive ion etching [22].

In this work, as was before mentioned, the photonic integrated circuits were fabricated with the use of this technique at UTT in France.

4.3 Silicon nitride nanophotonic platform for integrated quantum devices

Silicon nitride (Si_3N_4) waveguides have been used since 1970 as ultra-low loss planar waveguides. It is compatible with other platforms based on silicon technologies [50].

Si_3N_4 is a material that has enabled a large field for the fabrication of integrated devices as another platforms like silicon-on-insulator [23] and SiO_2 [51]. This material was used traditionally in the fabrication of CMOS platform circuits [52]. It is considered because low propagation losses and high refractive index allowing high confinement, which means a high scalability in the integration of this kind of circuits in a range for a few nanometers devices. Another remarkable points for Si_3N_4 that makes it an interesting material are the following: it can be used for the creation of photon heralded sources using spiral waveguides or ring resonators due to the high non linearity allowing the integration of the generation of photons [41]; it can be adaptable with active elements enabling to perform re-configurable circuits, it means, manipulation of photons; detection at the end of the photonic circuit can be achieved because it allows compatibility with integrated detectors like nanowires. Finally this platform must be compatible with current technology, in this case for couple and uncouple light to the photonic device it is viable to use fiber or gratings [3].

All this properties makes Si_3N_4 a suitable material for the fabrication of complex photonics circuits with potential applications in biosensing or quantum optics experiments, and more importantly, they are a suitable platform for quantum computing technologies which are of great interest in the recent years.
Nowadays, Si_3N_4 is used as platform for photonic technologies applied in lasers, biosensing, optical filters, optical signal processors, delay lines, optical frequency combs generation, supercontinuum generation, microfluidic and more applications [52].

For this reasons, we selected Si_3N_4 material for the design of our photonic integrated circuits.

4.3.1 Optical properties of silicon nitride (Si_3N_4)

The principal property of Si_3N_4 is the high refractive index of 2.1 in the near infrared. Also has low losses in the near and mid infrared. Those properties make it an interesting a suitable material for development of technology across the telecom band [53].

This material possesses a high third order nonlinearity, for the present work, we restricted only to the linear refractive index for the design and fabrication of our photonic circuits.

4.3.2 EBL: pattern transfer into e-beam resist

As we described above, the process of electron beam lithography, in the figure 4.2 is shown the schematic representation of the full process of manufacture.

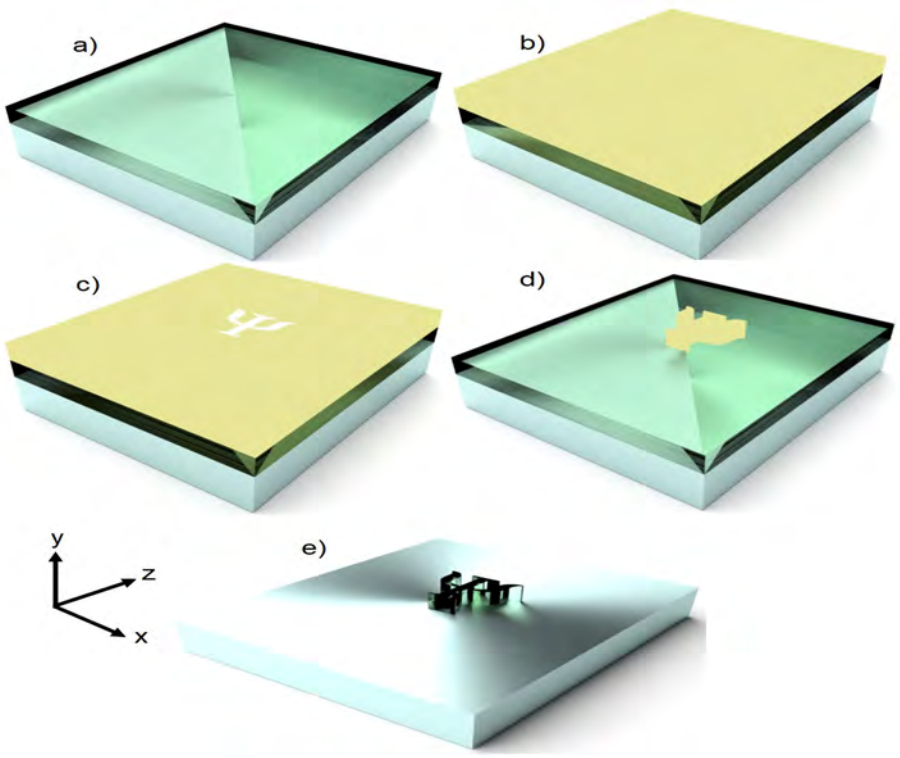

Figure 4.2: Schematic representation of the full process of electron beam lithography for the nanofabrication of nanostructures: a) The sample with a thin film of Si_3N_4, b) Deposition of the ebeam resist with spin coating technique. c) Pattern exposure to the electron beam. d) Development of the sample to remove the exposed resist and e) reactive ion etching process for the transfer of the pattern to the Si_3N_4 thin film.

The samples consist of a coverslip with a thickness of 170 μm with a thin film of Si_3N_4 with a thickness of 300 nm. Then the ebeam resist is deposited with the use of spin-coating technique. The resist reacts to the electron beam then, the pattern is generated and placed, such that the electron beam is focused on the top surface of the resist for the writing process.

After exposure, the sample is developed to remove the unexposed resist and finally, the pattern is transferred to the Si_3N_4 with the use of reactive ion etching technique.

4.3.2.1 Pattern generation, GDSII file

In order to create the nanophotonic circuits we need to generate a pattern that will be transferred to the sample along the full process of fabrication described below.

For the generation of the pattern for each device, I wrote Matlab scripts that generates the script for the use in the *CNST Nanolithography Toolbox* [54]. This tool is freely available and offers many basic structures for the creation of photonic circuits with different level of complexity, depending of the requirements of every user. It can be used to create

pattern layouts for nanoelectromechanical systems and nanophotonic devices. In addition, it is used for the creation of pattern for micro-devices. This software generates a GDSII file, which is used by the EBL system to transfer the pattern into the resist.

Once the device is completely designed another problem arises: How the light is going to be injected into the photonic circuits?. The first proposal to inject light into the photonic circuit was to inject the light using fiber to connect with the input waveguides with dimensions of 3 μm by 300 nm and then connect them with the nanophotonic circuit of interest with tappers with an adiabatic transition of light. Following the last consideration, all the circuits were designed with tapers and inputs waveguides with the dimensions before mentioned. All the devices have input ports that are designed with a separation to each other of 50 μm, so that allows to collect light in the photonic circuit selectively and decreasing the coupling in the curved zones.

We designed in 5 samples the following circuits: straight waveguides, directional couplers, CNOT Gates, and the photonic lattices of waveguides for the quantum simulators of quantum coherent transport of states, Glauber-Fock States and Bloch oscillations. In figure 4.3, we present the layouts we generated. In the same figure, f) layout is shown the central region for the quantum simulator of Bloch oscillations as a comparative with the previous designs.

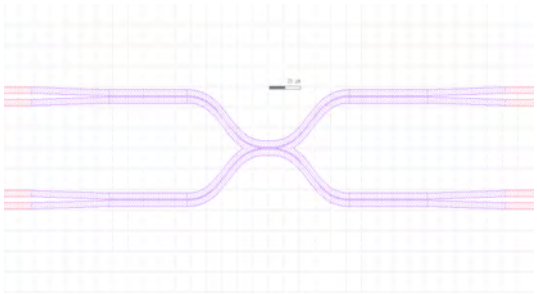

(a) Directional coupler.

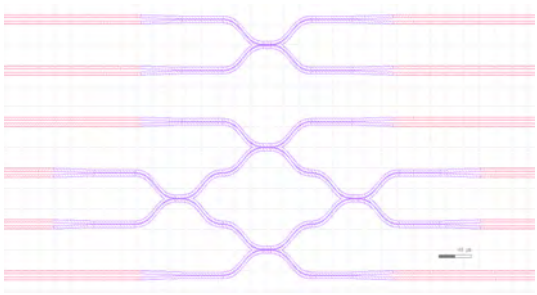

(b) CNOT gate.

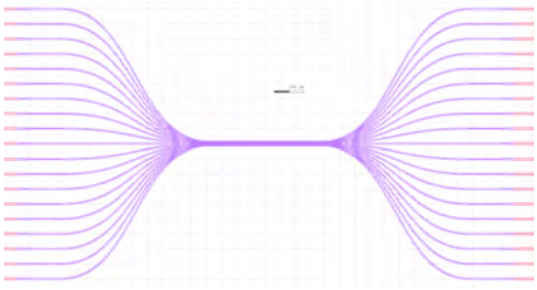

(c) Coherent quantum transport of states.

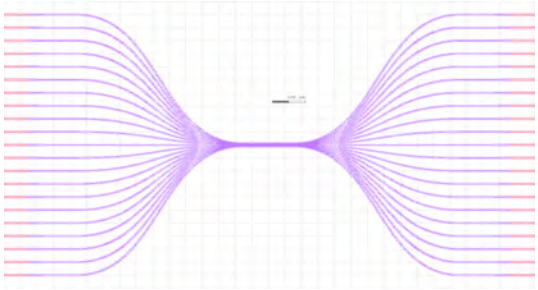

(d) Glauber-Fock sates.

(e) Bloch oscillations.

(f) Central zone of Bloch oscillations lattice

Figure 4.3: GDSII designs for integrated photonic circuits. All the patterns have dimensions around a few microns.

These are the shapes imported to the software that controls the electron beam lithography.

4.3.2.2 Preparation of the sample

Previously to the e-beam lithography process is necessary to prepare the sample. The following steps are required to obtain the best quality of the sample for the process.

- **Cleaning**: The samples were cleaned using isopropanol alcohol and acetone to remove dust particles, then the sample were dried with a nitrogen gun.

- **Resist deposition**: Using spin-coating technique, we deposited two layers with a constant velocity of 4000 rpm during 60 s. In both cases, this process involves a quick deposit to avoid the chemicals fluids dry. The first layer was the adhesion promoter AR300-80, we deposited a few drops in the center of the sample to obtain a homogeneous layer. The second layer was the positive e-beam resist AR-P 6200.09 during 60 s where the last process was repeated.

- **Annealing process**: After the deposition of the e-beam resist, the sample was annealed in a oven for 30 min at a temperature of 150 °C.

- **Deposition of the conductive layer**: Finally the last step is the deposition a film of conductive layer using spin-coating technique. The parameters of duration and velocity where the same last described. Due to Si_3N_4 is a dielectric material it can not distribute the charge leading to charge accumulation in the surface, this conductive layer helps to dissipate the charge.

All these layers deposited previously to electron beam lithography process are of so much importance, since if in some step the layer was not correctly deposited, the full process has to be done again.

4.3.2.3 Exposition parameters and development

When the sample is finally prepared, we introduced the sample into the electron beam microscope (eLINE Raith). The following parameters were used for the exposure:

Parameter	Value
Electron High Tension	20 kV
Aperture	10 μm
Beam Current	25 pA
Working Distance	8 mm
Area Dose	50 μC/ cm^2

Table 4.1: Exposure parameters in the electron beam lithography process.

We focused the electron beam on top surface of the resist surface in order to obtain a 20-nm-wide spot size. Furthermore, we corrected all possibles sources of aberrations related to the electron beam.
The e-beam can write over a surface of 100 μm by 100 μ with any sample displacement. Because our waveguides are grater that this write field, the sample is displaced with a motorized stage. To minimize errors in the displacement of the stage, a correction step is necessary, correction step that is called stitching. The stitching correction is of great importance to obtain continuity in all the optical devices.

After exposition, the sample is developed as follows:

- The sample is submerged in deionized water during 15 s to remove the conductive layer.
- Then, the sample is submerged in the developer AR600 S46 during 60 s. This developer removes all the resist exposed to the electron beam and exposes the pattern in the sample.
- After the development, the sample is submerged in isopropyl alcohol that removes the developer and stops the process of development.
- Finally, the sample is dried with a nitrogen gun.

Previously to the reactive ion etching process the samples were observed with an optical microscope to corroborate the writing process and development were realized correctly. In the figure 4.4 are shown optical microscope images of directional couplers after development process.

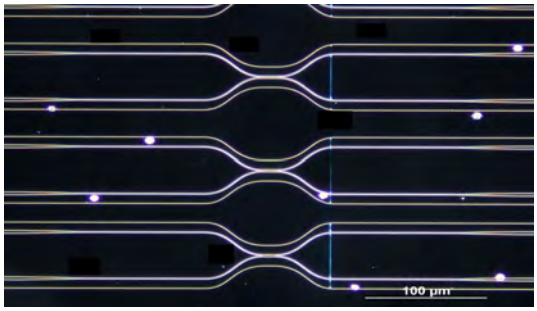

(a) Directional couplers with different separation distances and coupling lengths .

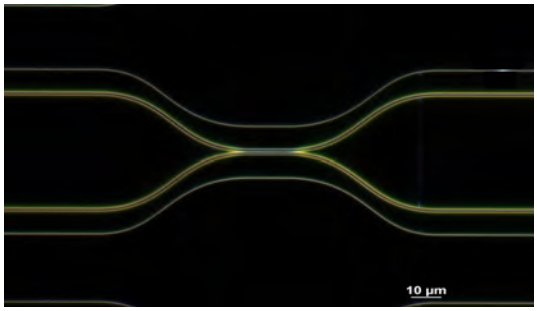

(b) Directional coupler.

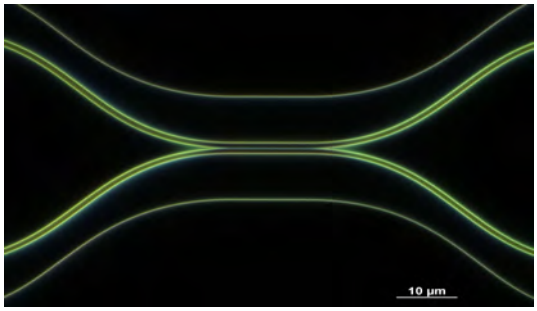

(c) Central region of a directional coupler.

Figure 4.4: Optical microscope images in dark field configuration after the process of development for directional couplers.

In the figure 4.5 are shown images of the CNOT gate after development process.

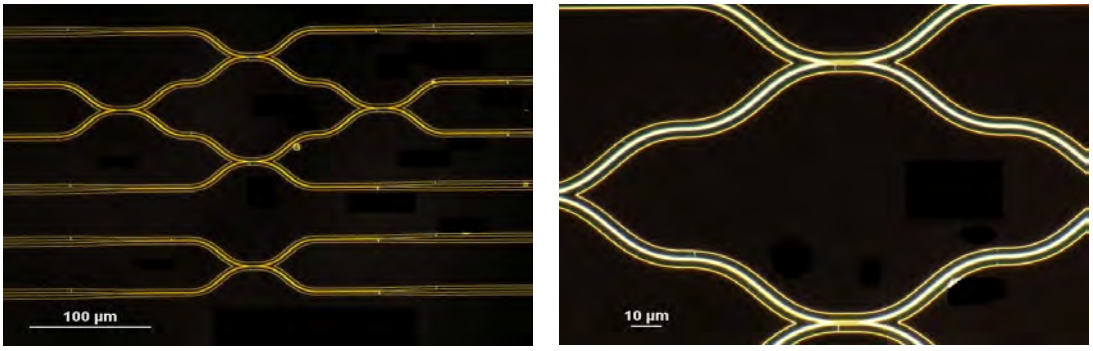

(a) CNOT gate. **(b) Magnification of the CNOT gate.**

Figure 4.5: Optical microscope images in dark field configuration after the process of development for CNOT gate.

In the figure 4.6 are shown images of the full photonic quantum simulator for quantum coherent transport of states and the central region where the optical waveguides are coupled.

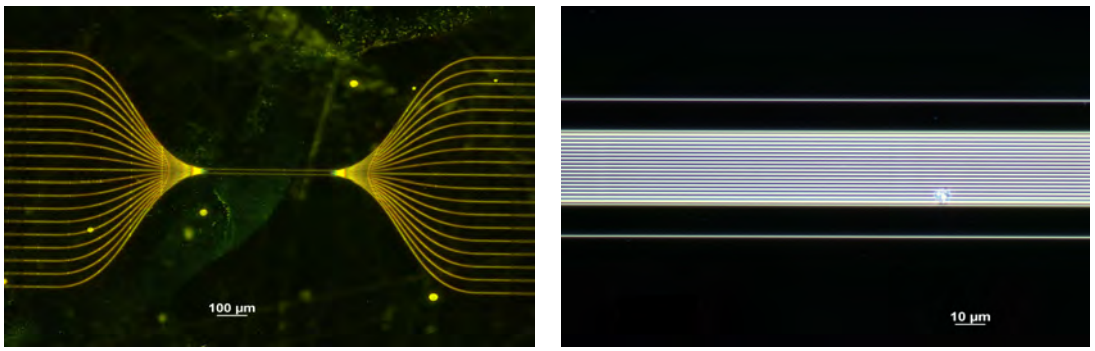

(a) Full image of the photonic circuit. **(b) Central zone of the photonic lattice where the waveguides are coupled.**

Figure 4.6: Optical microscope images in dark field configuration after the process of development for quantum coherent transport of states simulator.

In the figure 4.7 are shown images of the full photonic Glauber-Fock simulator and the central region where the optical waveguides are coupled, we can observe a small discontinuity due to the stitching correction.

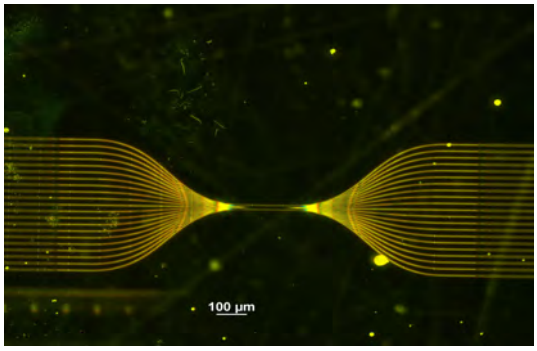

(a) Full image of the photonic circuit.

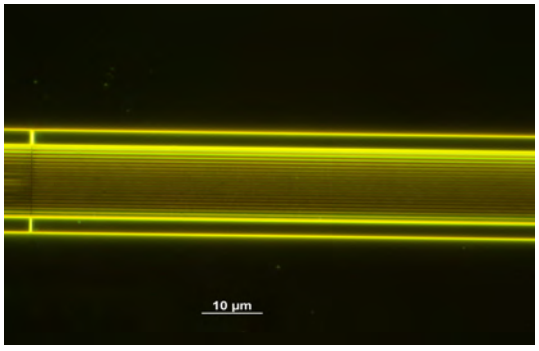

(b) Central zone of the photonic lattice where the waveguides are coupled.

Figure 4.7: Optical microscope images in dark field configuration after the process of development for Glauber-Fock photonic simulator.

In the figure 4.8 are shown images of the full photonic circuit for Bloch oscillations simulator, in the same way we observe a small discontinuity due to a failed stitching correction.

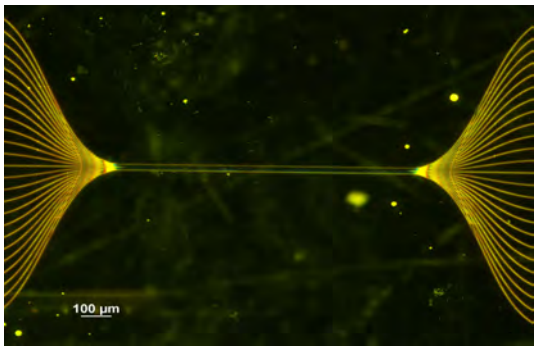

(a) Full image of the photonic circuit.

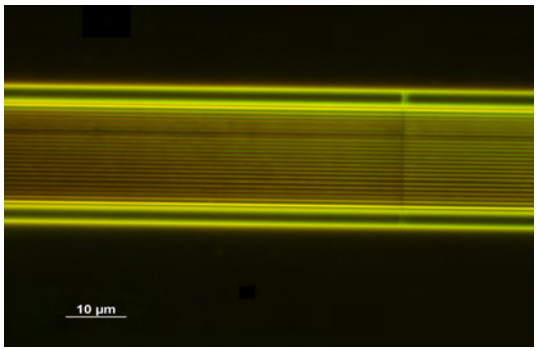

(b) Central zone of the photonic lattice where the waveguides are coupled.

Figure 4.8: Optical microscope images in dark field configuration after the process of development for Bloch oscillations simulator.

After development process to remove the resist, reactive ion etching is done in order to transfer the pattern into the silicon nitride. This process si described in the following subsection.

4.3.3 Reactive ion etching (RIE): pattern transfer into Si_3N_4

Reactive ion etching (RIE) is a type of plasma etch technology used in the fabrication of large scalable devices. A radio-frequency (RF) signal is applied so that an electric field ionizes the gas molecules and generates a plasma. The d.c. voltage extracts ions from the

plasma and energizes them and in the same way helps to the directionality of etching. For this reason the resist and Si_3N_4 starts to etch at different etch rates. Here, the etching process removes both materials the resist and the silicon nitride (Fig. 4.2). Because the etch rate of the resist is lower than that of the silicon nitride, the resist acts as a mask for the transfer of the pattern to the Si_3N_4 [55].
In Table 4.2, we present the parameters used for the RIE process.

Parameter	Value
Gas	CHF_3, 20 sccm
Pressure	5 m Torr
RIE power	100 W
Etch time	19 min

Table 4.2: Reactive ion etching parameters.

To remove the resist left at the end of the silicon nitride etching, we used oxygen plasma (O_2), with a flow of 10 sccm and pressure of 20 mTorr. The power of RF signal was selected to 10 W. Etch time was 1 min.

In the Fig. 4.9 are shown images of the CNOT gate after RIE process.

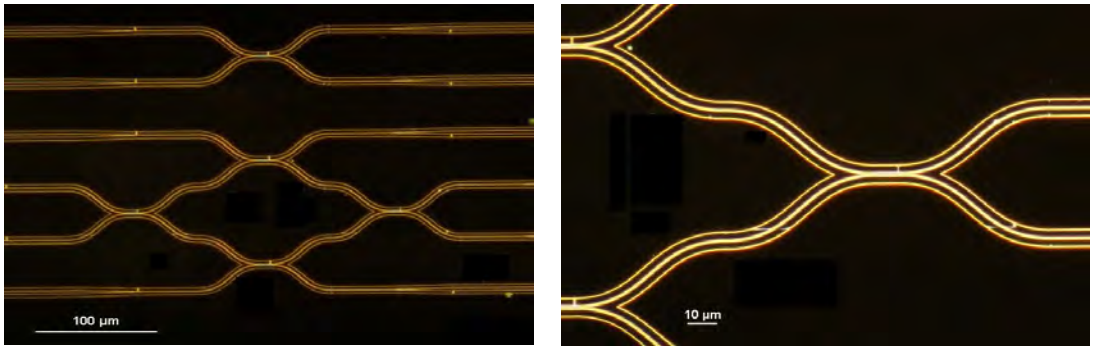

(a) CNOT gate. **(b) Magnification of the CNOT gate.**

Figure 4.9: Optical microscope images in dark field configuration after RIE process for the CNOT gate.

In the Fig. 4.10 are shown images of the full photonic quantum simulator for quantum coherent states and the central region where the optical waveguides are coupled.

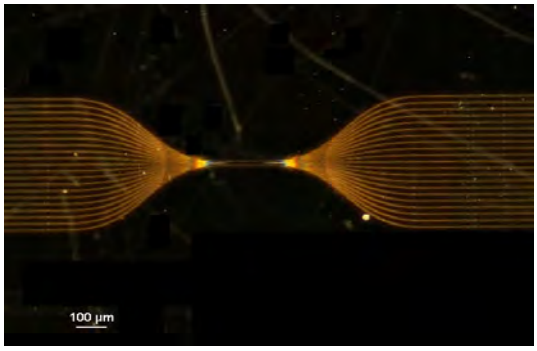

(a) Full image of the photonic circuit.

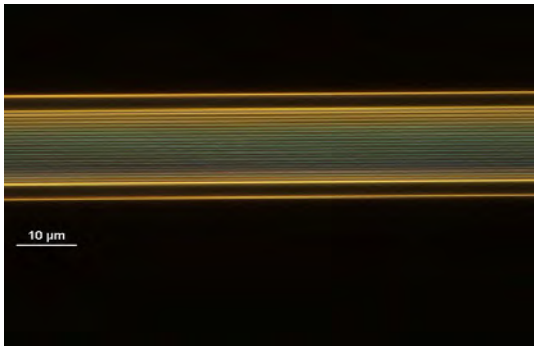

(b) Central zone of the photonic lattice where the waveguides are coupled.

Figure 4.10: Optical microscope images in dark field configuration after RIE process for quantum coherent transport of states simulator.

In the Fig. 4.11 are shown images of the full photonic Glauber-Fock simulator and the central region.

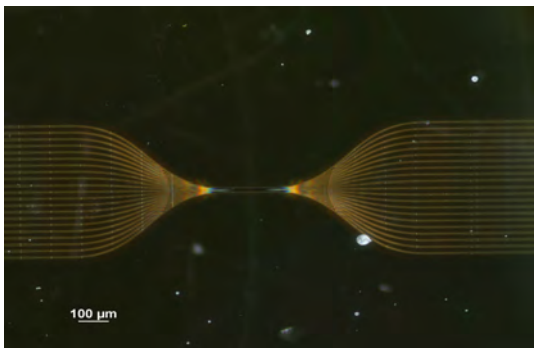

(a) Full image of the photonic circuit.

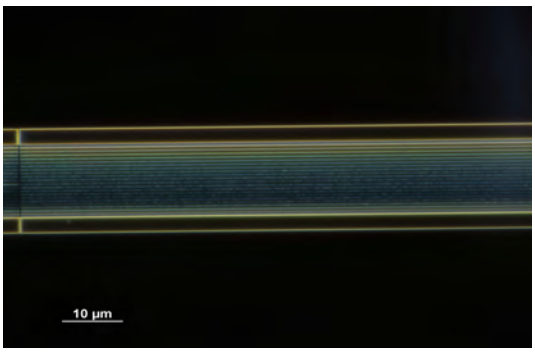

(b) Central zone of the photonic lattice where the waveguides are coupled.

Figure 4.11: Optical microscope images in dark field configuration after RIE for Glauber-Fock photonic simulator.

In the figure 4.12 are shown images of the full photonic circuit for Bloch oscillations simulator and the central region where the optical waveguides are coupled.

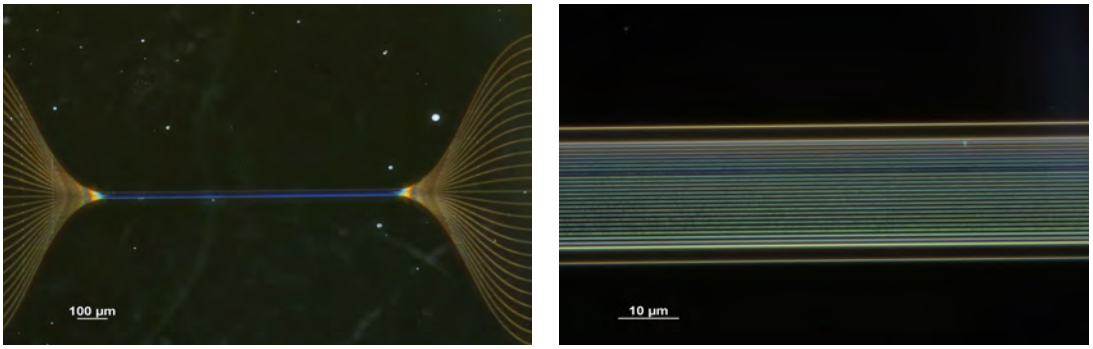

(a) Full image of the photonic circuit.

(b) Central zone of the photonic lattice where the waveguides are coupled.

Figure 4.12: Optical microscope images in dark field configuration after RIE process for Bloch oscillations simulator.

The last images shows the final result of the full process for nanofabrication of integrated photonic circuits. However, the optical microscope is limited by diffraction, which limits the measure of the integrated circuits. We observed the nanofabricated structures with scanning electron microscope (SEM) for higher resolution.

4.4 Nanofabrication results

In the present section, we show the principal result of this thesis related to the nanofabrication process. We present a few images of the principal integrated photonic circuits.

For SEM observation purposes, we spin-coated the sample with a conductive layer. The first sample was used to fabricate the devices and measure the width of them for a future correction. The width difference of the devices is around of 20 nm related with the spot size of the electron beam.

In the figure 4.13 are shown images of a directional coupler designed for the wavelength of 1550 nm, where the width expected was 1μm with a separation of 100 nm.

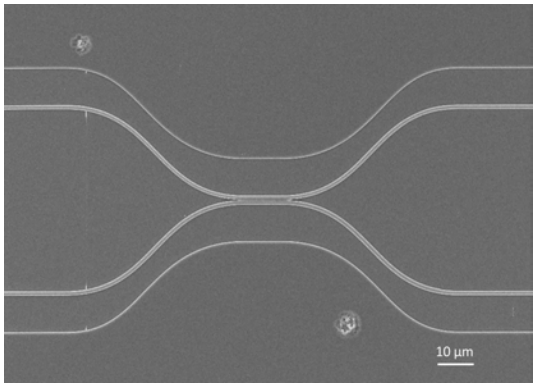

(a) Full image of directional coupler.

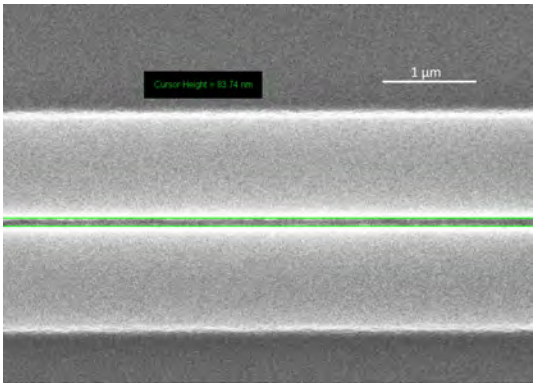

(b) Central zone of the directional coupler where the waeguides are closer to each other.

Figure 4.13: SEM images for the directional coupler for the wavelength of 1550 nm, designed with a separation of 100 nm.

In the Fig. 4.14 are shown images of the quantum simulator for quantum coherent transport, for the full device and the central zone where the optical waveguides are coupled.

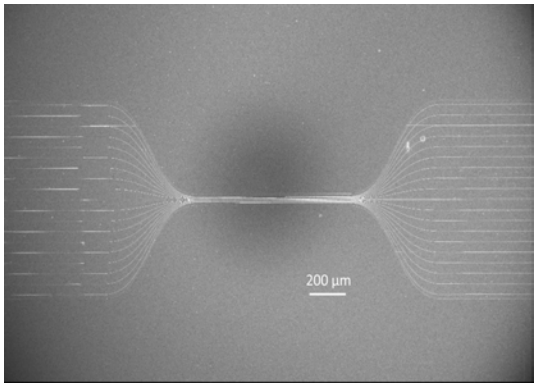

(a) Full image of the device.

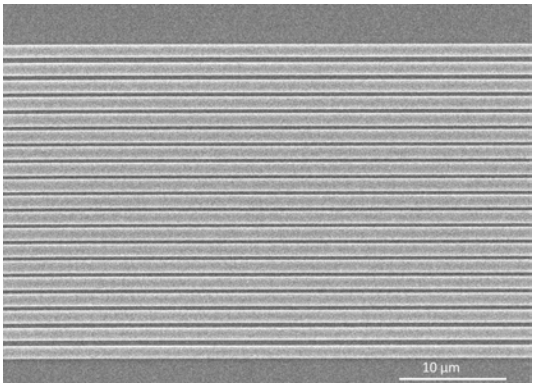

(b) Central zone of the photonic lattice where the waveguides are coupled.

Figure 4.14: SEM images for the photonic lattice for quantum coherent transport of states for the wavelength of $1550\ nm$.

In the figure 4.15 are shown images of the CNOT gate previously designed with different magnification. We observe there is not exist discontinuities due to the stitching correction.

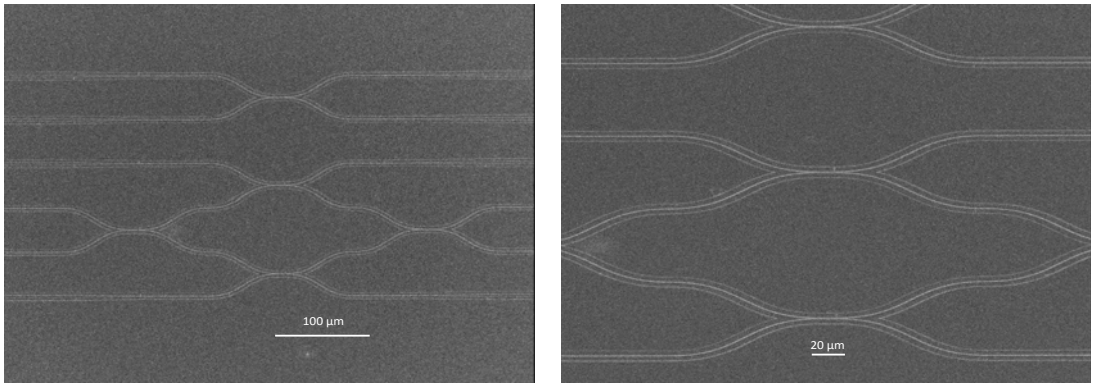

(a) Full image of CNOT gate.

(b) CNOT gate where only the central directional couplers are shown.

Figure 4.15: SEM images for the CNOT gate designed for the wavelength of $800\ nm$ with different magnification.

For all the optical devices SEM can be used in order to corroborate the fabrication process but long times of exposure of th devices relies on damage. For this reason we can not expose the circuits for long times or high magnification values.
These images have served to the characterization process. We just observed the photonic circuits have an increase of the width while the final length of them has maintained.

4.5 Conclusion

The process for the fabrication of nanophotonic circuits with the use of electron beam lithography technique was described. The process starts from the design of the mask layout particularly, we used the CNST nanolithography software. Then, the pattern is transferred to the resist with electron beam writing. Finally, the pattern is transferred to the Si_3N_4 thin-film with reactive ion etching process. We measured the width of the fabricated waveguides with scanning electron microscopy. Due to technology tolerances, we obtained a width increase of around of 20 nm, which we consider in subsequent process (i.e. decrease the layout).

Finally, making a comparison with femtosecond laser writing technique, we found electron beam lithography technique a suitable process for the fabrication of large-scalable nanophotonic circuits and more importantly, due to the optical properties of Si_3N_4, which is a material with so much optical properties that can be exploited in quantum technologies.

Chapter 5

Conclusion

In the present thesis, photonic quantum simulators were investigated theoretically, numerically, and experimentally with the development of a fabrication process. The main goal was to enable the photonic quantum simulators based on Si_3N_4 photonic platform, taking advantage of the optical properties of this material. The Heisenberg spin chain, Glauber-Fock states and Bloch oscillations were simulated in this platform, which allows the development of photonic nanowaveguides lattices. The principal advantage of this platform is the reduction of the footprint of about less than one millimeter, in contrast to femtosecond laser direct writing waveguides where the footprint is in the scale of centimeters. This compactness provides the key for the implementation of high-density photonic circuits.

We developed a theoretical and numerical study of the most important parameters that involves propagation of light in optical waveguides to simulate complex physical systems in solid-state physics, quantum computation and quantum optics.

WMM solver and Metric are powerful tools based on eigenmode expansion that allows the simulation of integrated photonic circuits with low computational requirements and time in comparison with other methods based on finite difference and finite element. This method reduces significantly the total time required for the development of integrated photonic circuits. In the same way, the evolution of light in optical lattices of waveguides was performed on this software in order to corroborate the desired dynamics in the optical arrays, previous to any fabrication process. In general, the use of Metric software allows the design of systems based on photonic waveguides to perform tasks for quantum technologies.

The research of the quantum simulator was developed considering just one photon at the input ports and just for the quantum coherent transport of states simulator we injected two photons: when two photons are considered in the photonic lattice, an interference pattern appears. This interference and the correlation function were not investigated in this work but can be studied in the future with possible applications.

For the quantum simulator of Bloch oscillations, we did not vary the input ports to observe the evolution of light, however this can be investigated in the future with the variation of the input ports. Furthermore, we can increase the propagation constant or modify the function of the propagation constant related to the potential energy as in solid-state physics.

Here, we considered and investigated the influence of two important parameters: the propagation constant (related to the dimensions of the waveguides) and coupling coefficient (related to the separation distance between the waveguides). With only these two parameters, we may implement and engineer other quantum system based on photonic quantum simulators.

Taking advantage of the large integration in a single chip of multiple integrated photonic circuits, we investigated and fabricated two fundamental gates for quantum computing science: directional couplers (Hadamard gate) and CNOT gates, both based on quantum interference of two indistinguishable photons.

Finally, we fabricated integrated nanophotonic circuits with the use of electron beam lithography. We chose silicon nitride (Si_3N_4) photonic platform due to its scalability in the integration process of many components on a single photonic chip. The high third-order susceptibility allows to foresee the implementation of integrated sources based nonlinear processes such as four-wave mixing. We foresee quantum photonic circuits with integrated generation and manipulation of single photons.

The integrated photonic circuits, fabricated during this Master thesis, constitute the first nanophotonic devices fabricated within the framework of an international collaboration between CIO in Mexico and UTT in France. The full characterization and implementation of this photonic circuits could allow a great impact in technology development in Mexico.

5.1 Perspectives

The following points are of interest for improvement and development of integrated photonic circuits in the future.

- Use of another techniques in order to inject light in the integrated photonic circuits like Bragg gratings with a high coupling efficiency.

- Due to silicon nitride material possess a third order non-linear susceptibility, it is possible to integrate photon pairs-sources in order to perform the generation and manipulation of photons in a single chip.

  In the figure 5.1 is shown a photon source that generates indistinguishable photons which contemplates a recent thesis of a student working in CICESE under a similar project of research with Université de Technologie de Troyes.

- Using this platform for fabrication is suitable the design of integrated photonic circuits with high complexity to develop a certain problem as boson sampling, quantum walks, disorder in photonic lattices, Anderson localization.

- Research how affects the interaction with the first and second neighbor in optical waveguide arrays and study of the dynamics.

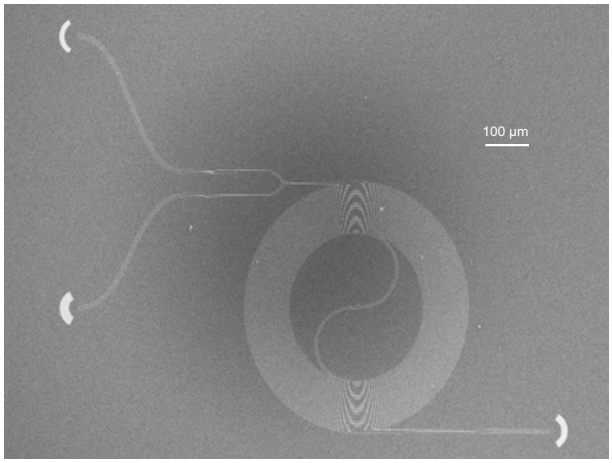

Figure 5.1: SEM images of an integrated photon pair source based on spontaneous four wave mixing on silicon nitride photonic platform. As a perspective, we plan to include the source and the photonic waveguide lattice in a single device.

- Research the correlation function and the pattern intereference due to the excitation with two photons in optical waveguide arrays.
- Research and simulation of the coupling constant between waveguides fabricated with laser writing and waveguides fabricated with electron beam technique for the performing of micro-nano waveguides connection.
- Integration of nanowires in order to perform the step of detection in the same chip.

Appendix A

Appendix

A.1 Appendix

In this appendix are described the process for the reduction of the ridge waveguide to planar waveguide and the mathematical description for the planar waveguide in order to find the solution for the TE mode and the correspondent effective index.

A.1.1 Planar waveguides

For this kind of waveguides also known as *Slab waveguides* we consider a Cartesian coordinates system and a medium with a profile of step-index for the refractive index, the electromagnetic waves oscillating only in one direction, for this case $x-axis$. Generally, the electric field and magnetic field are orthogonal to the direction of propagation ($z-axis$) in the form:

$$\tilde{\mathbf{E}}(\mathbf{r},t) = \vec{E}\,(x,y)\,e^{i(\omega t-\beta z)} \tag{A.1}$$

$$\tilde{\mathbf{H}}(\mathbf{r},t) = \vec{H}\,(x,y)\,e^{i(\omega t-\beta z)} \tag{A.2}$$

For the equation A.1 and A.2, i denotes the imaginary unity, ω is the frequency of the wave and the propagation constant represented with β.

Substituting equations A.1 and A.2 in the equations 2.7 and 2.8 and considering the refractive index constant, we find the wave equation for the electric field A.3 and the wave equation A.4 for the magnetic field:

$$\nabla_T^2\vec{E}\,(x,y) + (k_0^2n^2 - \beta^2)\vec{E}\,(x,y) = 0 \tag{A.3}$$

$$\nabla_T^2\vec{H}\,(x,y) + (k_0^2n^2 - \beta^2)\vec{H}\,(x,y) = 0 \tag{A.4}$$

Where $\nabla_T^2 = \frac{\partial^2}{\partial x^2} + \frac{\partial^2}{\partial y^2}$, correspond to the transversal laplacian operator and k_0 is the wavenumber in vacuum.

In order to solve the wave equation for the slab waveguide we assume the electric field

oscillates in the $x - direction$, and considering the orthogonality of the fields, it means, $\vec{E}(x, y) = E_y(x)$ for the electric field and $\vec{H}(x, y) = H_y(x)$ for the magnetic field.

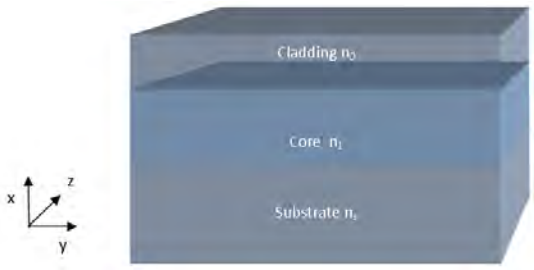

Figure A.1: Schematic image of a planar waveguide.

Taking into considerations the last assumptions and using the equation A.3 and A.4 we obtain the wave equation A.5 for the TE mode and the equation A.6 for the TM mode respectively.

$$\frac{d^2 E_y}{dx^2} + \left(k^2 n^2 - \beta^2\right) E_y = 0 \tag{A.5}$$

$$\frac{d^2 H_y}{dx^2} + \left(k^2 n^2 - \beta^2\right) H_y = 0 \tag{A.6}$$

In order to find the solution for a slab waveguide, we are going to solve only the TE modes.

- **TE modes** Considering the electric field oscillating in the core and exponentially decaying in the cladding, we propose the solutions described in the equation A.7, where the distribution of the refracive index is shown in the image A.2:

$$E_y = \left\{ \begin{array}{c} A\cos\left(\kappa a - \varphi\right) e^{-\sigma(x-a)} \\ A\cos\left(\kappa x - \varphi\right) \\ \text{A } \cos\left(\kappa a + \varphi\right) e^{\xi(x+a)} \end{array} \right\} \tag{A.7}$$

  The electromagnetic field with the exponential decaying out of the core is receives the name of evanescent waves, this waves depends of the refractive index of the substrate, the refractive index of cladding and the size of the waveguides

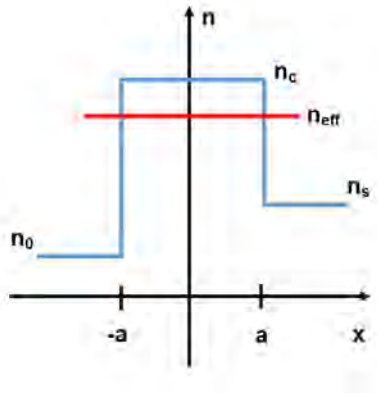

Figure A.2: Refractive index profile for a planar waveguide.

Where the constant used in the equation A.7 are defined with the following relations shown in the equation A.8:

$$\left\{ \begin{array}{l} \kappa^2 = \ k^2 n_1^2 - \beta^2 = \frac{u^2}{a^2} \\ \sigma^2 = \ \beta^2 - k^2 n_0^2 = \frac{w'^2}{a^2} \\ \xi^2 = \beta^2 - k^2 n_0^2 = \frac{w^2}{a^2} \end{array} \right\} \tag{A.8}$$

In order to establish continuity in all the optical waveguide we need to achieve that the function described for the equation A.7 and the first order derivative be equal in the boundaries a and $-a$. Under a few steps of algebra we can find the following relations:

$$u = \frac{m\pi}{2} + \frac{1}{2} tan^{-1}\left(\frac{w'}{u}\right) + \ \frac{1}{2} tan^{-1}\left(\frac{w}{u}\right) \tag{A.9}$$

$$\varphi = \frac{m\pi}{2} - \frac{1}{2} tan^{-1}\left(\frac{w'}{u}\right) + \ \frac{1}{2} tan^{-1}\left(\frac{w}{u}\right) \tag{A.10}$$

The equation A.9 and A.10 make up a coupled system of equations and satisfy the following identities:

$$u^2 + w^2 = k^2 a^2 \left(n_1^2 - n_0^2\right) = \nu^2 \tag{A.11}$$

$$w'^2 = \ \gamma \nu^2 + w^2 \tag{A.12}$$

$$\gamma = \frac{n_s^2 - n_0^2}{n_1^2 - n_s^2} \tag{A.13}$$

The parameter γ is related with the symmetry of the waveguide.

It is possible to make a transformation for the equation A.9 and A.10 to obtain a new equation. Defining the effective index through the equation A.14 as the refractive index that experiences a certain wavelength in the optical waveguide in the following way:

$$n_{eff} = \frac{\beta}{k} \tag{A.14}$$

Rewriting the normalized propagation constant with the equation A.15, we obtain:

$$b = \frac{n_{eff}^2 - n_s^2}{n_1^2 - n_s^2} \tag{A.15}$$

Finally, we can rewrite the equation shown in the equation A.16. This equation is normally called *Dispersion Equation or Trascendental Equation of Guided Modes* can be solved numerically with the refractive index of the core, the wavelength and the size of the waveguide.

$$2\nu\sqrt{1-b} = m\pi + tan^{-1}\left(\sqrt{\frac{b}{1-b}}\right) + tan^{-1}\left(\sqrt{\frac{b+\gamma}{1-b}}\right) \tag{A.16}$$

Solving the equation A.16 for a known value of ν it is possible to find the normalized propagation constant and then, find the effective refractive index in the waveguide.

The parameter m represent the order of the mode in the optical waveguide, when $m = 0$, it is known as *fundamental mode.*

When we find the effective refractive index, all the parameters are known for the equation A.7, just rest to determine the amplitude of the electric field which is provided by the intensity of the electric field.

It is possible to follow the same procedure for the TM modes to obtain the dispersion equation for the guided modes.

A.1.2 Silicon Nitride Photonic Waveguides

The Silicon Nitride (Si_3N_4) is a material that has enabled a large field for the manufacture of integrated devices as another platforms like Silicon on Insulator [23], or SiO_2 [51]. This material was used traditionally in manufacture of CMOS platform circuits [52]. is considered because low propagation losses and high refractive index allowing high confinement, which means a high scalability in the integration of this kind of circuits in a range for a few nanometers devices.

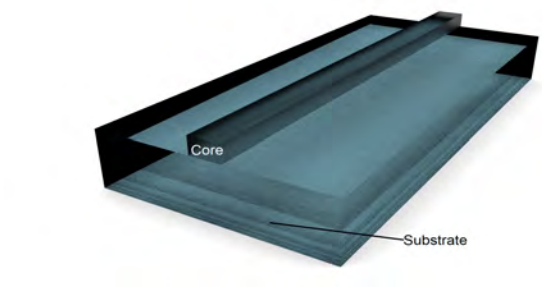

Figure A.3: Schematic representation of a Si_3N_4 ridge waveguide.

Another remarkable points for Si_3N_4 that make it as an interesting material are the following: it can be used for the creation of photon heralded sources using spiral waveguides or ring resonators due to the high non linearity allowing the integration of the generation of photons [41]; it can be adaptable with active elements enabling to perform re-configurable circuits, it means, manipulation of photons; detection at the end of the photonic circuit can be achieved because it allows compatibility with integrated detectors like nano-wires.

Finally this platform must be compatible with actual technology, in this case for couple and uncouple light to the photonic device it is viable to use fiber or gratings [3].

All this properties makes Si_3N_4 a suitable material for the manufacture of complex photonics circuits with potential applications in biosensing or quantum optics experiments, and more importantly, they are a suitable platform for quantum computing technologies which are of great interest in the recent years.

A.1.3 Effective Index Method

For the simulation of a three dimensional structure in a software becomes in long times and many resources for computational data, it is possible to reduce the complexity of this problem if we simulates only a two dimensional structure, it means, we can propagate light in the original direction of propagation in a slab waveguide with the same width [27].

In the figure A.4 is shown a ridge waveguide that can be divided in three region in the vertical direction, for all the regions we can calculate the effective refrative index, region I and III are the same, such that region are going to have the same effective refractive index while in region II can we solve as a slab waveguide.

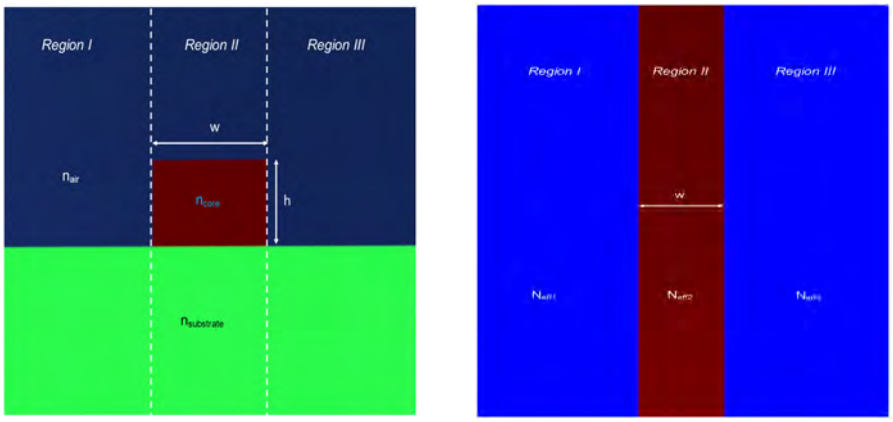

(a) XY-Plane of a ridge waveguide. **(b) Slab waveguide reduced.**

Figure A.4: Effective index method used for the reduction of a ridge waveguide to a slab waveguide.

Using last assumption enables a more easy treatment of photonic waveguides reducing resources and time in the computing step for simulation.

Bibliography

[1] Fulvio Flamini, Lorenzo Magrini, Adil S Rab, Nicolò Spagnolo, Vincenzo D'ambrosio, Paolo Mataloni, Fabio Sciarrino, Tommaso Zandrini, Andrea Crespi, Roberta Ramponi, et al. Thermally reconfigurable quantum photonic circuits at telecom wavelength by femtosecond laser micromachining. *Light: Science & Applications*, 4(11):e354, 2015. 1, 3

[2] Andrea Crespi, Mirko Lobino, Jonathan CF Matthews, Alberto Politi, Chris R Neal, Roberta Ramponi, Roberto Osellame, and Jeremy L O'Brien. Measuring protein concentration with entangled photons. *Applied Physics Letters*, 100(23):233704, 2012. 1

[3] Simeon Bogdanov, MY Shalaginov, Alexandra Boltasseva, and Vladimir M Shalaev. Material platforms for integrated quantum photonics. *Optical Materials Express*, 7(1):111–132, 2017. 1, 45, 67

[4] Jonathan P Dowling and Kaushik P Seshadreesan. Quantum optical technologies for metrology, sensing, and imaging. *Journal of Lightwave Technology*, 33(12):2359–2370, 2015. 1

[5] Alán Aspuru-Guzik and Philip Walther. Photonic quantum simulators. *Nature Physics*, 8:285 EP –, 04 2012. 1

[6] R. Blatt and C.F. Roos. Quantum simulations with trapped ions. *Nature Physics*, 8:277, 2012. 1

[7] Thaddeus D Ladd, Fedor Jelezko, Raymond Laflamme, Yasunobu Nakamura, Christopher Monroe, and Jeremy Lloyd O'Brien. Quantum computers. *nature*, 464(7285):45, 2010. 1

[8] Jeremy L O'brien, Akira Furusawa, and Jelena Vučković. Photonic quantum technologies. *Nature Photonics*, 3(12):687, 2009. 1

[9] Stefano Longhi. Quantum-optical analogies using photonic structures. *Laser & Photonics Reviews*, 3(3):243–261, 2009. 1

[10] A Perez-Leija, H Moya-Cessa, and DN Christodoulides. Optical realization of the atom–field interaction in waveguide lattices. *Physica Scripta*, 2012(T147):014023, 2012. 3

[11] Hao Tang, Xiao-Feng Lin, Zhen Feng, Jing-Yuan Chen, Jun Gao, Ke Sun, Chao-Yue Wang, Peng-Cheng Lai, Xiao-Yun Xu, Yao Wang, et al. Experimental two-dimensional quantum walk on a photonic chip. *Science advances*, 4(5):eaat3174, 2018. 3

[12] Alberto Peruzzo, Mirko Lobino, Jonathan CF Matthews, Nobuyuki Matsuda, Alberto Politi, Konstantinos Poulios, Xiao-Qi Zhou, Yoav Lahini, Nur Ismail, Kerstin Wörhoff, et al. Quantum walks of correlated photons. *Science*, 329(5998):1500–1503, 2010. 3

[13] Armando Perez-Leija, Robert Keil, Alastair Kay, Hector Moya-Cessa, Stefan Nolte, Leong-Chuan Kwek, Blas M Rodríguez-Lara, Alexander Szameit, and Demetrios N Christodoulides. Coherent quantum transport in photonic lattices. *Physical Review A*, 87(1):012309, 2013. 3, 21

[14] Robert Keil, Armando Perez-Leija, Felix Dreisow, Matthias Heinrich, Hector Moya-Cessa, Stefan Nolte, Demetrios N Christodoulides, and Alexander Szameit. Classical analogue of displaced fock states and quantum correlations in glauber-fock photonic lattices. *Physical review letters*, 107(10):103601, 2011. 3

[15] Stefano Longhi. Optical realization of the two-site bose–hubbard model in waveguide lattices. *Journal of Physics B: Atomic, Molecular and Optical Physics*, 44(5):051001, 2011. 3

[16] WeiFeng Zhang, Xiao Zhang, Yaroslav V Kartashov, Xianfeng Chen, and Fangwei Ye. Bloch oscillations in arrays of helical waveguides. *Physical Review A*, 97(6):063845, 2018. 3, 22, 39

[17] Ye-Long Xu, William S Fegadolli, Lin Gan, Ming-Hui Lu, Xiao-Ping Liu, Zhi-Yuan Li, Axel Scherer, and Yan-Feng Chen. Experimental realization of bloch oscillations in a parity-time synthetic silicon photonic lattice. *Nature communications*, 7:11319, 2016. 3, 22, 39

[18] Lane Martin, Giovanni Di Giuseppe, Armando Perez-Leija, Robert Keil, Felix Dreisow, Matthias Heinrich, Stefan Nolte, Alexander Szameit, Ayman F Abouraddy, Demetrios N Christodoulides, et al. Anderson localization in optical waveguide arrays with off-diagonal coupling disorder. *Optics express*, 19(14):13636–13646, 2011. 3

[19] Andrea Crespi, Roberto Osellame, Roberta Ramponi, Vittorio Giovannetti, Rosario Fazio, Linda Sansoni, Francesco De Nicola, Fabio Sciarrino, and Paolo Mataloni. Anderson localization of entangled photons in an integrated quantum walk. *Nature Photonics*, 7(4):322, 2013. 3

[20] K. M. Davis, K. Miura, N. Sugimoto, and K. Hirao. Writing waveguides in glass with a femtosecond laser. *Optics Letters*, 21:1729–1731, 1996. 3, 43

[21] Huan Huang, Lih Mei Yang, and Jian Liu. Femtosecond fiber laser direct writing of optical waveguide in glasses. *SPIE*, 81640B, 2011. 3

[22] C Vieu, F Carcenac, A Pepin, Y Chen, M Mejias, A Lebib, L Manin-Ferlazzo, L Couraud, and H Launois. Electron beam lithography: resolution limits and applications. *Applied surface science*, 164(1-4):111–117, 2000. 3, 44

[23] M Bruel. Silicon on insulator material technology. *Electronics letters*, 31(14):1201–1202, 1995. 3, 45, 66

[24] Joshua W Silverstone, Damien Bonneau, Jeremy L O'Brien, and Mark G Thompson. Silicon quantum photonics. *IEEE Journal of Selected Topics in Quantum Electronics*, 22(6):390–402, 2016. 3

[25] Jianwei Wang, Stefano Paesani, Yunhong Ding, Raffaele Santagati, Paul Skrzypczyk, Alexia Salavrakos, Jordi Tura, Remigiusz Augusiak, Laura Mančinska, Davide Bacco, et al. Multidimensional quantum entanglement with large-scale integrated optics. *Science*, 360(6386):285–291, 2018. 3

[26] Yogesh N Joglekar, Clinton Thompson, Derek D Scott, and Gautam Vemuri. Optical waveguide arrays: quantum effects and pt symmetry breaking. *The European Physical Journal-Applied Physics*, 63(3), 2013. 3, 22, 23, 39

[27] Katsunari Okamoto. *Fundamentals of Optical Waveguides*. Academic Press, 2006. 7, 8, 67

[28] Ginés Lifante. *Integrated Photonics: Fundamentals*. Wiley, 2003. 7, 8, 10

[29] John. D. Joannnopoulus, Steven G. Johnson, Joshua N. Winn, and Robert D. Meade. *Photonic crystals: molding the flow of light*. Princeton University press, 2008. 9, 10

[30] Amnon Yariv. *Quantum Electronics*. Wiley, 1989. 10

[31] Amnon Yariv. Coupled-mode theory for guided-wave optics. *IEEE Journal of Quantum Electronics*, 9(9):919–933, 1973. 10, 23

[32] Alexander Szameit, Felix Dreisow, Thomas Pertsch, Stefan Nolte, and Andreas Tünnermann. Control of directional evanescent coupling in fs laser written waveguides. *Optics Express*, 15(4):1579–1587, 2007. 10

[33] Yann G Boucher. Analytical model for the coupling constant of a directional coupler in terms of slab waveguides. *Optical Engineering*, 53(7):071810–071810, 2014. 10

[34] O. V. Ivanova, M. Hammer, R. Stoffer, and E. van Groesen. A variational mode expansion mode solver. *Optical and Quantum Electronics*, 39(10):849–864, 2007. 12

[35] Metric website. Introduction and general remarks. https://metric.computational-photonics.eu/general.html. 12

[36] Christopher Gerry, Peter Knight, and Peter L Knight. *Introductory quantum optics*. Cambridge University press, 2005. 13, 17

[37] Robert Keil. *Quantum random walks in waveguide lattices*. PhD thesis, Universität Jena, 2013. 15

[38] Roy J Glauber. Coherent and incoherent states of the radiation field. *Physical Review*, 131(6):2766, 1963. 16

[39] Chong-Ki Hong, Zhe-Yu Ou, and Leonard Mandel. Measurement of subpicosecond time intervals between two photons by interference. *Physical review letters*, 59(18):2044, 1987. 17

[40] Linda Sansoi. *Integrated devices for quantum information with polarization encoded qubits*. PhD thesis, Sapienza Universitá di ROma, 2012. 17

[41] Alberto Politi, Martin J Cryan, John G Rarity, Siyuan Yu, and Jeremy L O'brien. Silica-on-silicon waveguide quantum circuits. *Science*, 320(5876):646–649, 2008. 20, 45, 67

[42] Andrea Crespi, Roberta Ramponi, Roberto Osellame, Linda Sansoni, Irene Bongioanni, Fabio Sciarrino, Giuseppe Vallone, and Paolo Mataloni. Integrated photonic quantum gates for polarization qubits. *Nature communications*, 2:566, 2011. 20

[43] Sougato Bose. Quantum communication through an unmodulated spin chain. *Physical review letters*, 91(20):207901, 2003. 21

[44] P Alsing, D-S Guo, and HJ Carmichael. Dynamic stark effect for the jaynes-cummings system. *Physical Review A*, 45(7):5135, 1992. 21

[45] Robert Keil, Armando Perez-Leija, Felix Dreisow, Matthias Heinrich, Hector Moya-Cessa, Stefan Nolte, Demetrios N Christodoulides, and Alexander Szameit. Classical analogue of displaced fock states and quantum correlations in glauber-fock photonic lattices. *Physical review letters*, 107(10):103601, 2011. 21

[46] J Feldmann, K Leo, Jagdeep Shah, DAB Miller, JE Cunningham, T Meier, G Von Plessen, A Schulze, P Thomas, and S Schmitt-Rink. Optical investigation of bloch oscillations in a semiconductor superlattice. *Physical Review B*, 46(11):7252, 1992. 22

[47] Brian P Anderson and Ma A Kasevich. Macroscopic quantum interference from atomic tunnel arrays. *Science*, 282(5394):1686–1689, 1998. 22

[48] Giacomo Corrielli, Andrea Crespi, Giuseppe Della Valle, Stefano Longhi, and Roberto Osellame. Fractional bloch oscillations in photonic lattices. *Nature communications*, 4:1555, 2013. 22

[49] Ajoy Ghatak K. Thyagarajan. *Introduction to Fiber Optics*. Cambridge University Press, 1998. 23

[50] W Stutius and W Streifer. Silicon nitride films on silicon for optical waveguides. *Applied Optics*, 16(12):3218–3222, 1977. 45

[51] Jeremy O'Brien, Alberto Politi, Graham d. Marshall, Jonathan C.F. Matthews, Peter Dekker, Martin Ams, and Michael J. Withford. Laser written waveguide photonic quantum circuits. *Optics Express*, 17(15):12546–12554, 2009. 45, 66

[52] Chris GH Roeloffzen, Leimeng Zhuang, Caterina Taddei, Arne Leinse, René G Heideman, Paulus WL van Dijk, Ruud M Oldenbeuving, David AI Marpaung, Maurizio Burla, and Klaus-J Boller. Silicon nitride microwave photonic circuits. *Optics express*, 21(19):22937–22961, 2013. 45, 66

[53] Kevin Luke, Yoshitomo Okawachi, Michael RE Lamont, Alexander L Gaeta, and Michal Lipson. Broadband mid-infrared frequency comb generation in a si$_3$n$_4$ microresonator. *Optics letters*, 40(21):4823–4826, 2015. 45

[54] Krishna C Balram, Daron A Westly, Marcelo Davanco, Karen E Grutter, Qing Li, Thomas Michels, Christopher H Ray, Liya Yu, Richard J Kasica, Christopher B Wallin, et al. The nanolithography toolbox. *Journal of Research of the National Institute of Standards and Technology*, 121:464–476, 2016. 46

[55] Shinichi Tachi, Kazunori Tsujimoto, and Sadayuki Okudaira. Low-temperature reactive ion etching and microwave plasma etching of silicon. *Applied physics letters*, 52(8):616–618, 1988. 53